

REMOVING SPURIOUS CONCEPTS FROM NEURAL NETWORK REPRESENTATIONS VIA JOINT SUBSPACE ESTIMATION

Floris Holstege^{1,2}, Bram Wouters¹, Noud van Giersbergen¹, Cees Diks^{1,2}

¹University of Amsterdam, Department of Quantitative Economics ²Tinbergen Institute

{f.g.holstege, b.m.wouters, n.p.a.vanGiersbergen, c.g.h.diks}@uva.nl

ABSTRACT

Out-of-distribution generalization in neural networks is often hampered by spurious correlations. A common strategy is to mitigate this by removing spurious concepts from the neural network representation of the data. Existing concept-removal methods tend to be overzealous by inadvertently eliminating features associated with the main task of the model, thereby harming model performance. We propose an iterative algorithm that separates spurious from main-task concepts by jointly identifying two low-dimensional orthogonal subspaces in the neural network representation. We evaluate the algorithm on benchmark datasets for computer vision (Waterbirds, CelebA) and natural language processing (MultiNLI), and show that it outperforms existing concept removal methods.

1 INTRODUCTION

Deep neural networks (DNNs) are typically trained to optimize their performance on a given dataset, but this criterion rarely captures the ability of a model to generalize to out-of-distribution (OOD) data. A key reason for this is that the model relies on spurious correlations (Gururangan et al., 2018; Srivastava et al., 2020; Wang & Culotta, 2020; Sagawa et al., 2020; Zhou et al., 2021). For example, if a model’s main task is to distinguish between images of cows and penguins, the training data might contain a spurious correlation between animal type and background (cows typically appear on grasslands, penguins on snow). The model could exploit this correlation by basing its main-task classification on the background (Geirhos et al., 2020). As a consequence, its performance deteriorates if the background is no longer correlated with the animal type in the OOD data.

For tabular data, one can simply remove a variable if deemed spurious. However, removing spurious correlations directly from images or text is non-trivial and costly. An alternative is to focus on the embeddings, which are vector representations generated by the neural network of images or text. Post-hoc concept-removal methods aim to eliminate a concept from the embeddings, after the neural network has been trained. A *concept* refers to a representation in the data of a human-defined object or phenomenon (Kim et al., 2018). In the example of distinguishing cows and penguins, the background type is the *spurious concept*. Typically the parameters of the neural network are frozen and a concept classifier is trained on the embeddings, from which the concept features are then removed (Ravfogel et al., 2020; 2022a). Afterwards, a linear classifier is trained on the transformed embeddings to predict the *main-task concept* (e.g. animal type) and thereby preventing the model from using the spurious concept for main-task classification.

A drawback of post-hoc removal methods is that they also tend to remove main-task features from the embeddings, because due to the spurious correlation main-task features can be used to predict the spurious concept. For example, a concept classifier might use the cow’s horns to predict a grassland background. As a result, removing these features hurts the main-task performance of the model (Ravfogel et al., 2020; Belinkov, 2022; Kumar et al., 2022).

Our contribution¹: this paper improves on current post-hoc concept-removal methods by separating spurious and main-task concepts in the embedding space. We do so by jointly identifying two

¹Code can be found at <https://github.com/fholstege/JSE-replicate>

low-dimensional orthogonal subspaces, one associated with the spurious concept (e.g. background) and the other with the main-task concept (e.g. animal type). This crucially differs from existing methods, which only focus on the spurious concept features, risking the loss of vital main-task information. Furthermore, we make the identification of the subspaces systematic by introducing statistical tests that attribute directions in the embedding space to either the main-task or the spurious concept. The method, which we call Joint Subspace Estimation (JSE), is shown to be robust against the strength of the spurious correlation and to outperform existing concept-removal methods for a Toy dataset as well as benchmark datasets for image recognition (Waterbirds, CelebA) and natural language processing (MultiNLI). A high-level overview of the method is given in Figure 1.

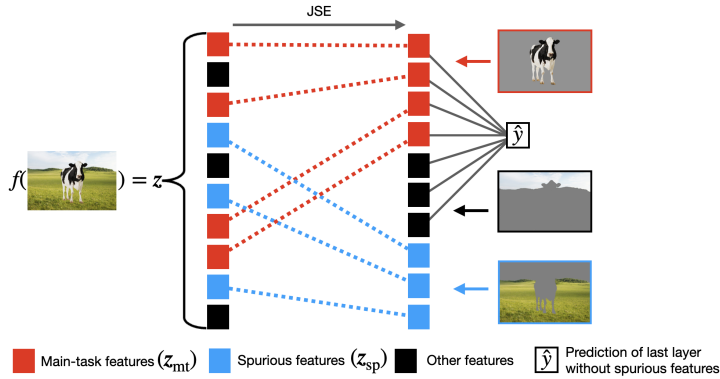


Figure 1: **High-level overview of Joint Subspace Estimation (JSE) for concept removal:** the input x is fed through a neural network $f(x)$, from which we can extract the vector representation z . Within the vector representation, two orthogonal subspaces are identified: one related to the *spurious concept* (the background), and one to the *main-task concept* (bird type). JSE estimates the subspaces of the two concepts simultaneously to prevent mixing of spurious and main-task features.

2 SPURIOUS CORRELATIONS, OOD GENERALIZATION & CONCEPT REMOVAL

We consider the random variables $\mathcal{D} = (y_{mt}, y_{sp}, \mathbf{x})$, where $y_{mt} \in \{0, 1\}$ is the main-task concept label, $y_{sp} \in \{0, 1\}$ is the spurious concept label and $\mathbf{x} \in \mathcal{X}$ represents the input features. Each input \mathbf{x} contains subsets \mathbf{x}_{mt} and \mathbf{x}_{sp} of features corresponding to the main-task and spurious concept, respectively. In the example of cows and penguins, \mathbf{x}_{mt} and \mathbf{x}_{sp} correspond to the pixels showing the animal and the background. It is assumed that \mathbf{x}_{mt} and \mathbf{x}_{sp} are non-overlapping subsets and causally determine the associated labels y_{mt} and y_{sp} , respectively (see Figure 2):

$$p(y_{mt}, y_{sp}, \mathbf{x}_{mt}, \mathbf{x}_{sp}) = p(y_{mt}|\mathbf{x}_{mt}) p(y_{sp}|\mathbf{x}_{sp}) p(\mathbf{x}_{mt}, \mathbf{x}_{sp}). \quad (1)$$

This implies $p(y_{mt}|\mathbf{x}) = p(y_{mt}|\mathbf{x}_{mt})$, but it does not mean that the main-task label y_{mt} and the spurious features \mathbf{x}_{sp} are independent; they can be dependent due to dependence between \mathbf{x}_{mt} and \mathbf{x}_{sp} . Since they are not causally related, we say they are spuriously correlated. At the level of trained neural networks, this means that a main-task classifier tends to make use of the spurious features \mathbf{x}_{sp} within \mathbf{x} . Previous work offers a number of possible reasons, ranging from stochastic gradient descent (SGD) training dynamics (Pezeshki et al., 2021) and overparameterization (Sagawa et al., 2020; D’Amour et al., 2020) to inductive biases of DNNs (Rahaman et al., 2019).

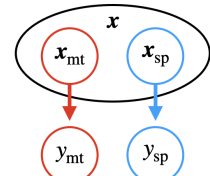


Figure 2: **Causal relation between features and labels**

Let $p_{\text{train}}(\cdot)$ denote the distribution for the training data, and $p_{\text{OOD}}(\cdot)$ the distribution for OOD data. The problem of OOD generalization arises when the trained DNN is applied to data that has a different dependence between main-task and spurious features (i.e. the $p_{\text{train}}(\mathbf{x}_{mt}, \mathbf{x}_{sp}) \neq p_{\text{OOD}}(\mathbf{x}_{mt}, \mathbf{x}_{sp})$, while the conditionals and all marginal distributions remain the same). This generally leads to $p_{\text{train}}(y_{mt}|\mathbf{x}_{sp}) \neq p_{\text{OOD}}(y_{mt}|\mathbf{x}_{sp})$. Since the trained DNN uses spurious features to predict the main-task label, this shift in the conditional distribution may lead to a deterioration of performance. To be more concrete, a penguin in a grassland background will be classified as a cow.

We now restrict our analysis to DNNs for classification, which typically consist of a complicated function $f(\mathbf{x}) : \mathcal{X} \rightarrow \mathbb{R}^d$ mapping the input features to a vector representation, followed by a linear

layer. We assume the embedding vectors $z \in \mathbb{R}^d$ have a similar structure as the input features \mathbf{x} , in the sense that each z has non-overlapping subsets $z_{\text{mt}} \in \mathcal{Z}_{\text{mt}} \subseteq \mathbb{R}^d$ and $z_{\text{sp}} \in \mathcal{Z}_{\text{sp}} \subseteq \mathbb{R}^d$ that causally determine the labels y_{mt} and y_{sp} , respectively. It should be stressed that this does not necessarily hold, as the trained DNN could have mixed main-task and spurious features because of their predictive ability for the main-task label y_{mt} . However, there is recent empirical evidence that even when trained on data with a spurious correlation, neural networks tend to learn both main-task and spurious features (Kirichenko et al., 2023; Izmailov et al., 2022; Rosenfeld et al., 2022).

In addition, we assume that \mathcal{Z}_{mt} and \mathcal{Z}_{sp} are linear subspaces of the embedding space \mathbb{R}^d . This sometimes goes under the name of *linear subspace hypothesis* (Bolukbasi et al., 2016; Vargas & Cotterell, 2020). Previous work shows that linear subspaces can encode information about complex concepts (Bau et al., 2017; Alain & Bengio, 2017). Moreover, non-linear information about the spurious concept cannot be used by the last layer for binary classification (Ravfogel et al., 2023).

One concept-removal approach to the problem of OOD generalization is to project the embedding vectors $z \in \mathbb{R}^d$ onto a linear subspace, before feeding it to the final linear layer. Suppose that $\mathbf{v}_{\text{sp},1}, \mathbf{v}_{\text{sp},2}, \dots, \mathbf{v}_{\text{sp},d_{\text{sp}}}$ is an orthonormal basis of the spurious embedding subspace $\mathcal{Z}_{\text{sp}} \subseteq \mathbb{R}^d$ and \mathbf{V}_{sp} is the matrix ($d \times d_{\text{sp}}$) whose columns are the basis vectors. Then the transformation from z to $(\mathbf{I} - \mathbf{V}_{\text{sp}}\mathbf{V}_{\text{sp}}^T)z$ is the orthogonal projection onto the orthogonal complement of $\mathbb{R}^d \setminus \mathcal{Z}_{\text{sp}}$ and thereby removes the spurious features from the representation. A linear layer that uses the transformed embeddings to predict the binary main-task label y_{mt} will therefore not use the spurious concept and model performance will not be affected when applied to OOD data.

In practice, however, it is highly non-trivial to estimate (a basis of) the subspace \mathcal{Z}_{sp} . Due to the spurious correlations, classifiers that use the embedding vectors to predict the spurious label y_{sp} also make use of the main-task embeddings z_{mt} . As a consequence, an estimate of \mathcal{Z}_{sp} will also contain directions that are actually part of \mathcal{Z}_{mt} . Projecting out the estimate of \mathcal{Z}_{sp} removes main-task information and therefore hurts the performance of the resulting main-task classifier (Ravfogel et al., 2020; Belinkov, 2022; Kumar et al., 2022). We will see that our JSE method addresses this problem by estimating not only \mathcal{Z}_{sp} , but also the main-task embedding space \mathcal{Z}_{mt} .

2.1 RELATED WORK

Spurious correlations: The problem of neural networks relying on spurious correlations has arisen in both computer vision (Geirhos et al., 2019; Xiao et al., 2021; Singla & Feizi, 2022) and NLP (Niven & Kao, 2019; Kaushik & Lipton, 2018; McCoy et al., 2019). There is a wide range of methods addressing spurious correlations in neural networks, including data augmentation (Hermann et al., 2020), invariant learning (Arjovsky et al., 2019; Ahuja et al., 2021), or instance reweighing (Sagawa et al., 2020; Idrissi et al., 2022). A specific set of methods focuses on the last layer of the DNN, by re-training it on a dataset in which the main-task and spurious concept labels are balanced (Kirichenko et al., 2023). This addresses the case where $p_{\text{train}}(y_{\text{mt}}|y_{\text{sp}}) \neq p_{\text{OOD}}(y_{\text{mt}}|y_{\text{sp}})$, but not the problem of $p_{\text{train}}(y_{\text{mt}}|\mathbf{x}_{\text{sp}}) \neq p_{\text{OOD}}(y_{\text{mt}}|\mathbf{x}_{\text{sp}})$ (Puli et al., 2022, see also Appendix E).

Concept-removal methods: Concept removal is mainly based on adversarial approaches (Goodfellow et al., 2014), commonly to mitigate undesirable biases (Edwards & Storkey, 2016; Zhang et al., 2018; Wang et al., 2021). This is frequently referred to as adversarial removal (ADV). However, the ability of ADV to remove concepts has been called into question (Elazar & Goldberg, 2018). An alternative is to remove a linear subspace from the embeddings (Bolukbasi et al., 2016; Ethayarajh et al., 2019; Dev & Phillips, 2019; Dev et al., 2021). A key method in this category is iterative null-space projection (INLP, Ravfogel et al., 2020), in which a linear classifier predicts the concept labels, and the coefficients of the classifier are orthogonally projected from the embeddings. This is repeated until the concept cannot be predicted. A follow-up method is relaxed linear adversarial concept erasure (RLACE), in which an orthogonal projection matrix is trained such that the concept cannot be predicted from the embeddings (Ravfogel et al., 2022a).

3 JOINT SUBSPACE ESTIMATION

We will now introduce Joint Subspace Estimation (JSE) in which the spurious and main-task embedding subspaces \mathcal{Z}_{sp} and \mathcal{Z}_{mt} are estimated simultaneously. The method will be discussed in three steps. Section 3.1 explains how to simultaneously estimate individual basis vectors for \mathcal{Z}_{sp} and

\mathcal{Z}_{mt} . Section 3.2 introduces an iterative procedure to find multiple basis vectors for \mathcal{Z}_{sp} and \mathcal{Z}_{mt} . Section 3.3 puts forward two statistical tests to terminate the iterative procedure and to determine the dimensions of \mathcal{Z}_{sp} and \mathcal{Z}_{mt} .

3.1 ESTIMATING SPURIOUS AND MAIN-TASK CONCEPT VECTORS

As a starting point, consider simultaneously estimating one vector $\mathbf{v}_{\text{sp}} \in \mathcal{Z}_{\text{sp}}$ and another vector $\mathbf{v}_{\text{mt}} \in \mathcal{Z}_{\text{mt}}$. A usual approach for estimating \mathbf{v}_{sp} is to train a logistic regression on the embeddings, $\hat{y}_{\text{sp}} = \text{Logit}^{-1}(\mathbf{z}^T \mathbf{w}_{\text{sp}} + b_{\text{sp}})$, and then to use the (normalized) coefficients $\mathbf{v}_{\text{sp}} = \mathbf{w}_{\text{sp}} / \|\mathbf{w}_{\text{sp}}\|$ as a so-called concept vector \mathbf{v}_{sp} that contains information about the concept (Kim et al., 2018). However, if we perform logistic regression in a sample where the spurious and main-task features are correlated, then the estimate of \mathbf{v}_{sp} might have components in the direction of main-task features (and vice versa for the estimate of \mathbf{v}_{mt}). To address this issue, we need to assume a relation between the two subspaces, which is done by the following assumption.

Orthogonality Assumption. *The linear subspaces \mathcal{Z}_{sp} and \mathcal{Z}_{mt} are orthogonal, i.e. each vector $\mathbf{v}_{\text{sp}} \in \mathcal{Z}_{\text{sp}}$ is perpendicular to each vector $\mathbf{v}_{\text{mt}} \in \mathcal{Z}_{\text{mt}}$.*

It should be noted that this assumption is consistent with the earlier assumption of the features determining the labels y_{sp} and y_{mt} being distinct, and the empirical observation that high-level concepts are distinctly represented in the embeddings (Kirichenko et al., 2023). Also note that orthogonality does not imply independence between main-task and spurious features, as was additionally assumed in earlier work (Chen et al., 2020).

The idea behind the orthogonality assumption is that it discourages the estimate of \mathbf{v}_{sp} to use main-task features, as it is forced to be perpendicular to a main-task direction \mathbf{v}_{mt} , and vice-versa. We illustrate the effect of the assumption in Figures 3 panels A and D for Toy data, and analyse how JSE is affected when the orthogonality assumption does not hold in Appendix B. An alternative perspective on the orthogonality assumption is that we are trying to identify subspaces of \mathcal{Z}_{sp} and \mathcal{Z}_{mt} that are orthogonal to each other and that are most informative about the respective labels. If \mathcal{Z}_{sp} and \mathcal{Z}_{mt} are high-dimensional (which is the case in most realistic settings), the idea is that these subspaces cover significant parts of \mathcal{Z}_{sp} and \mathcal{Z}_{mt} in terms of their ability to predict y_{sp} and y_{mt} .

We thus simultaneously perform a logistic regression on the embeddings \mathbf{z} for y_{sp} and y_{mt} , subject to the constraint of orthogonality of \mathbf{w}_{sp} and \mathbf{w}_{mt} . This means that for a sample $\{y_{\text{mt},i}, y_{\text{sp},i}, \mathbf{z}_i\}_{i=1}^n$ we perform the following optimization,

$$\hat{\mathbf{w}}_{\text{sp}}, \hat{\mathbf{w}}_{\text{mt}}, \hat{b}_{\text{sp}}, \hat{b}_{\text{mt}} = \underset{\substack{\mathbf{w}_{\text{sp}}, \mathbf{w}_{\text{mt}}, b_{\text{sp}}, b_{\text{mt}} \\ (\mathbf{w}_{\text{sp}} \perp \mathbf{w}_{\text{mt}})}}{\arg \min} \sum_{i=1}^n \mathcal{L}_{\text{BCE}}(\hat{y}_{\text{sp},i}, y_{\text{sp},i}) + \mathcal{L}_{\text{BCE}}(\hat{y}_{\text{mt},i}, y_{\text{mt},i}), \quad (2)$$

where \mathcal{L}_{BCE} is the binary cross-entropy (BCE). Furthermore, $\hat{y}_{\text{sp},i} = \text{Logit}^{-1}(\mathbf{z}_i^T \mathbf{w}_{\text{sp}} + b_{\text{sp}})$, and similarly for $\hat{y}_{\text{mt},i}$. The estimated spurious and main-task concept vectors are then $\hat{\mathbf{v}}_{\text{sp}} = \hat{\mathbf{w}}_{\text{sp}} / \|\hat{\mathbf{w}}_{\text{sp}}\|$ and $\hat{\mathbf{v}}_{\text{mt}} = \hat{\mathbf{w}}_{\text{mt}} / \|\hat{\mathbf{w}}_{\text{mt}}\|$.

3.2 ITERATIVELY ESTIMATING MULTIPLE CONCEPT AND MAIN-TASK VECTORS

The concept subspaces \mathcal{Z}_{sp} and \mathcal{Z}_{mt} will generally not be one-dimensional. As a consequence, the estimated spurious concept vector $\hat{\mathbf{v}}_{\text{sp}}$ could still contain main-task components (and vice versa for $\hat{\mathbf{v}}_{\text{mt}}$). To address this, we propose an iterative procedure to estimate orthonormal bases of the subspaces \mathcal{Z}_{sp} and \mathcal{Z}_{mt} , which are guaranteed to be orthogonal to each other.

For now, let us focus on estimating a vector $\mathbf{v}_{\text{sp}} \in \mathcal{Z}_{\text{sp}}$. By applying the procedure of Equation 2 gives a $\hat{\mathbf{v}}_{\text{sp}}$ and $\hat{\mathbf{v}}_{\text{mt}}$, where $\hat{\mathbf{v}}_{\text{sp}}$ may still have components in \mathcal{Z}_{mt} and $\hat{\mathbf{v}}_{\text{mt}}$ may have components in \mathcal{Z}_{sp} . We propose to project out the direction $\hat{\mathbf{v}}_{\text{mt}}$ from the embeddings and to repeat the optimization of Equation 2 for the resulting subspace. Doing this multiple times will eventually remove all main-task information from the subspace, guaranteeing that the estimated vector $\hat{\mathbf{v}}_{\text{sp},1}$ is orthogonal to the (estimated) main-task subspace.

By projecting out $\hat{\mathbf{v}}_{\text{sp},1}$ from the original embeddings and repeating the whole procedure $d_{\text{sp}} = \dim(\mathcal{Z}_{\text{sp}})$ times, we estimate an orthonormal basis $\hat{\mathbf{v}}_{\text{sp},1}, \hat{\mathbf{v}}_{\text{sp},2}, \dots, \hat{\mathbf{v}}_{\text{sp},d_{\text{sp}}}$ of \mathcal{Z}_{sp} that is orthogonal to the (main-task) subspace. The method described is a nested for-loop (see Algorithm 1), where

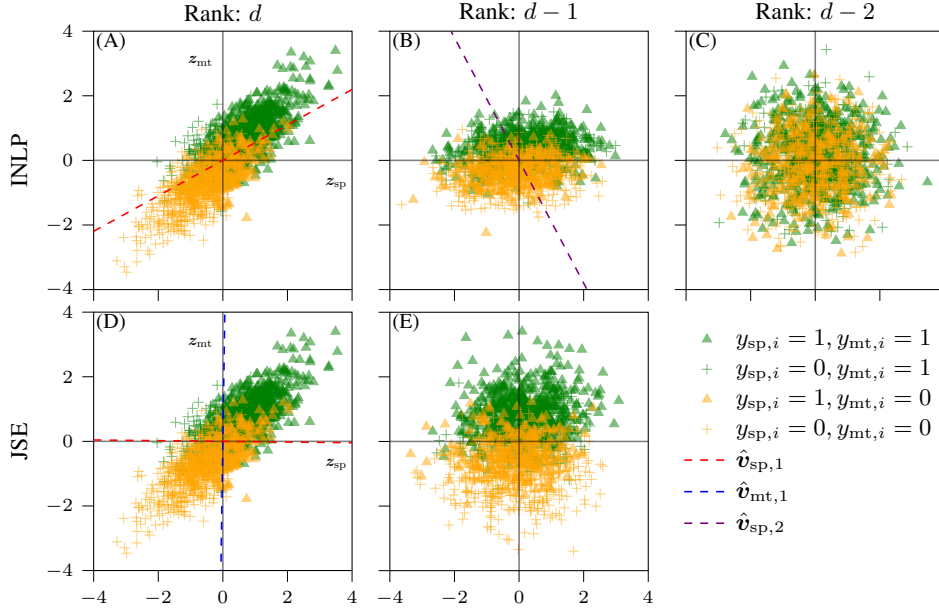


Figure 3: **Illustration of JSE, in comparison to INLP:** Based on the $d(=20)$ -dimensional Toy dataset of Section 4.1 with $\rho = 0.8$ and sample size $n = 2,000$. Two-dimensional slices of the embedding space before and after projecting out one (or multiple) spurious direction(s) are shown, as well as the identified main-task and spurious directions. Panels A and D have the spurious feature on the x-axis and the main-task feature on the y-axis. In the other panels the axes that best separate the main-task labels are shown.

the inner loop finds and projects out main-task vectors, and the outer loop finds and projects out spurious vectors. After having found the basis of \mathcal{Z}_{sp} , one can repeat the inner loop one last time to find $d_{\text{mt}} = \dim(\mathcal{Z}_{\text{mt}})$ vectors $\hat{\mathbf{v}}_{\text{mt},1}, \hat{\mathbf{v}}_{\text{mt},2}, \dots, \hat{\mathbf{v}}_{\text{mt},d_{\text{mt}}}$ constituting an estimated basis for \mathcal{Z}_{mt} . For a more detailed description of the algorithm, see Appendix C.

Algorithm 1 JSE algorithm to estimate orthonormal bases for \mathcal{Z}_{sp} and \mathcal{Z}_{mt} . The conditions in the **if**-statements are discussed in Section 3.3.

Require: a sample $\{y_{\text{mt},i}, y_{\text{sp},i}, \mathbf{z}_i\}_{i=1}^n$ consisting of two binary labels and a vector $\mathbf{z}_i \in \mathbb{R}^d$.

Initialize a $(n \times d)$ -dimensional embedding matrix $\mathbf{Z} = (\mathbf{z}_1 \mathbf{z}_2 \dots \mathbf{z}_n)^T$.

Initialize $\mathbf{Z}_{\text{sp}}^\perp \leftarrow \mathbf{Z}$.

for $i = 1, \dots, d$ **do**

$\mathbf{Z}_{\text{remain}} \leftarrow \mathbf{Z}_{\text{sp}}^\perp$

for $j = 1, \dots, d$ **do**

 Estimate $\hat{\mathbf{w}}_{\text{sp}}$ and $\hat{\mathbf{w}}_{\text{mt}}$ with Equation 2, using embeddings $\mathbf{Z}_{\text{remain}}$.

 Define normalized directions $\hat{\mathbf{v}}_{\text{sp},i} \leftarrow \hat{\mathbf{w}}_{\text{sp}} / \|\hat{\mathbf{w}}_{\text{sp}}\|$ and $\hat{\mathbf{v}}_{\text{mt},j} \leftarrow \hat{\mathbf{w}}_{\text{mt}} / \|\hat{\mathbf{w}}_{\text{mt}}\|$.

if $\hat{\mathbf{v}}_{\text{mt},j}$ is a proper main-task direction **then**

 Projection $\mathbf{Z}_{\text{remain}} \leftarrow \mathbf{Z}_{\text{sp}}^\perp (\mathbf{I} - \hat{\mathbf{V}}_{\text{mt}} \hat{\mathbf{V}}_{\text{mt}}^T)$, where $\hat{\mathbf{V}}_{\text{mt}} = (\hat{\mathbf{v}}_{\text{mt},1} \hat{\mathbf{v}}_{\text{mt},2} \dots \hat{\mathbf{v}}_{\text{mt},j})$.

else

break

end if

end for

if $\hat{\mathbf{v}}_{\text{sp},i}$ is a proper spurious direction **then**

 Projection $\mathbf{Z}_{\text{sp}}^\perp \leftarrow \mathbf{Z} (\mathbf{I} - \hat{\mathbf{V}}_{\text{sp}} \hat{\mathbf{V}}_{\text{sp}}^T)$, where $\hat{\mathbf{V}}_{\text{sp}} = (\hat{\mathbf{v}}_{\text{sp},1} \hat{\mathbf{v}}_{\text{sp},2} \dots \hat{\mathbf{v}}_{\text{sp},i})$.

else

break

end if

end for

return $\hat{\mathbf{v}}_{\text{sp},1}, \hat{\mathbf{v}}_{\text{sp},2}, \dots, \hat{\mathbf{v}}_{\text{sp},i}$

So far, we have treated the subspaces \mathcal{Z}_{sp} and \mathcal{Z}_{mt} equally. This symmetry is broken in Algorithm 1, as the main-task directions are identified in the inner loop and the concept directions in the outer loop. In Appendix C we give empirical evidence that swapping the inner and outer loop has little effect on the outcome of the JSE method. Furthermore, we show that training the linear classifier on \mathcal{Z}_{mt} instead of $\mathcal{Z}_{\text{sp}}^\perp$ gives similar performance.

3.3 TESTING WHEN TO STOP ADDING CONCEPT OR MAIN-TASK VECTORS

So far, in the description of the iterative algorithm we have assumed the dimensions d_{sp} and d_{mt} of the respective subspaces \mathcal{Z}_{sp} and \mathcal{Z}_{mt} to be known. In practice, the dimensions must be estimated via stopping criteria of the (nested) for loops in Algorithm 1. Let us focus on the condition in the outer loop: “ \mathbf{v}_{sp} is a proper spurious direction” for a given (normalized) direction $\mathbf{v}_{\text{sp}} \in \mathbb{R}^d$ in the embedding space. The condition in the inner loop is, *mutatis mutandis*, the same.

The statement “ \mathbf{v}_{sp} is a proper spurious direction” means that two criteria are both met:

1. **The direction \mathbf{v}_{sp} is informative about the spurious label y_{sp}** , meaning that the embeddings projected onto \mathbf{v}_{sp} are able to predict the spurious label. To be concrete, a logistic regression based on the projected embeddings should have a higher accuracy than an classifier that just predicts the majority class, which we refer to as a ‘random classifier’.
2. **The direction \mathbf{v}_{sp} should be more predictive of the spurious concept than of the main-task concept.** Due to the spurious correlation, a vector in \mathcal{Z}_{sp} is likely also predictive for the main-task concept. We nonetheless associate it with the spurious subspace \mathcal{Z}_{sp} , as long as its prediction accuracy for the spurious label is higher than for the main-task label.

Note that the first criterion is already used in Ravfogel et al. (2020), while the second is novel and addresses the problem of inadvertently removing main-task information in existing concept-removal methods. This is illustrated in Figure 3 (panel B), where the INLP-method of Ravfogel et al. (2020) removes a feature that is more predictive of the main-task concept than the spurious concept.

To make these criteria operational, we introduce two statistical tests in terms of differences between BCE’s. For the first criterion we compare the BCE of $\hat{y}_{\text{sp}}^{(\mathbf{v}_{\text{sp}})} = \text{Logit}^{-1}(\gamma_{\text{sp}} \mathbf{z}^T \mathbf{v}_{\text{sp}} + b_{\text{sp}})$, which is a predictor for the label y_{sp} based on the embeddings projected onto \mathbf{v}_{sp} , and the BCE of a majority-rule ‘random classifier’. The model parameters γ_{sp} and b_{sp} are to be trained by minimizing the BCE. For the second criterion we compare the BCE of $\hat{y}_{\text{sp}}^{(\mathbf{v}_{\text{sp}})}$ with the analogously defined $\hat{y}_{\text{mt}}^{(\mathbf{v}_{\text{sp}})}$, which is a predictor of y_{mt} . Both tests are performed using a t -statistic, using an equally weighted average of the BCE’s over the four combinations of y_{sp} and y_{mt} . For a precise definition of the hypotheses, test statistics, and their properties, see Appendix D.

4 EXPERIMENTS

In this section we apply our JSE procedure to a Toy dataset of embeddings, two vision datasets (Waterbirds, CelebA) and one NLP dataset (MultiNLI). We compare JSE with standard empirical risk minimization (ERM), which does not attempt to mitigate the problem of OOD generalization due to spurious correlations, and with the concept-removal methods mentioned in Section 2.1: iterative null-space projection (INLP), relaxed linear adversarial concept erasure (RLACE) and adversarial removal based on a single linear adversary (ADV). In Appendix E we compare our method against group-weighted ERM. We have done this separately, as this is not a concept-removal method. Details about the datasets, experimental setup and parameter selection can be found in Appendix F. For numerical details of the results, see Appendix A.

4.1 TOY DATASET

We create a Toy dataset of d -dimensional embeddings drawn from a multivariate normal distribution with a block correlation matrix,

$$\mathbf{z} \sim \mathcal{N}(\boldsymbol{\mu} = \mathbf{0}, \boldsymbol{\Sigma}), \quad \text{where} \quad \boldsymbol{\Sigma} = \begin{bmatrix} \boldsymbol{\Sigma}_{\text{sp,mt}} & \mathbf{0} \\ \mathbf{0} & \mathbf{I} \end{bmatrix}, \quad \boldsymbol{\Sigma}_{\text{sp,mt}} = \begin{bmatrix} 1 & \rho \\ \rho & 1 \end{bmatrix}.$$

Note that, unlike more realistic situations, the embeddings here are not neural network representations of underlying input features. We set \mathcal{Z}_{sp} and \mathcal{Z}_{mt} to be one-dimensional, with spurious and main-task directions given by $\mathbf{w}_{\text{sp}} = (\gamma_{\text{sp}}, 0, 0, \dots, 0)^T$ and $\mathbf{w}_{\text{mt}} = (0, \gamma_{\text{mt}}, 0, \dots, 0)^T$, respectively. We define binary labels y_{sp} and y_{mt} following a logit model,

$$p(y_{\text{sp}} = 1|\mathbf{z}) = \text{Logit}^{-1}(\mathbf{z}^T \mathbf{w}_{\text{sp}} + b_{\text{sp}}), \quad p(y_{\text{mt}} = 1|\mathbf{z}) = \text{Logit}^{-1}(\mathbf{z}^T \mathbf{w}_{\text{mt}} + b_{\text{mt}}).$$

Throughout the simulations we take $d = 20$, $b_{\text{sp}} = b_{\text{mt}} = 0$ and $\gamma_{\text{sp}} = \gamma_{\text{mt}} = 3$. In this setup the parameter ρ is the correlation between the spurious and main-task features, thereby determining the spurious relation $p_{\text{train}}(y_{\text{mt}}|\mathbf{z}_{\text{sp}})$ between the main-task label and the spurious feature.

Figure 3 illustrates the functioning of JSE and compares it with INLP. It shows two-dimensional slices of the embedding space before and after projecting out one (or multiple) spurious direction(s). JSE identifies the main-task and spurious directions nearly perfectly (panel D). Furthermore, the procedure terminates after one projection, as the remaining class separation is attributed to the main-task concept (panel E). INLP identifies (superpositions of) the main-task and spurious directions both as spurious (panels A, B). Virtually all main-task information is inadvertently removed from the remaining ($d - 2 = 18$)-dimensional embedding space (panel C).

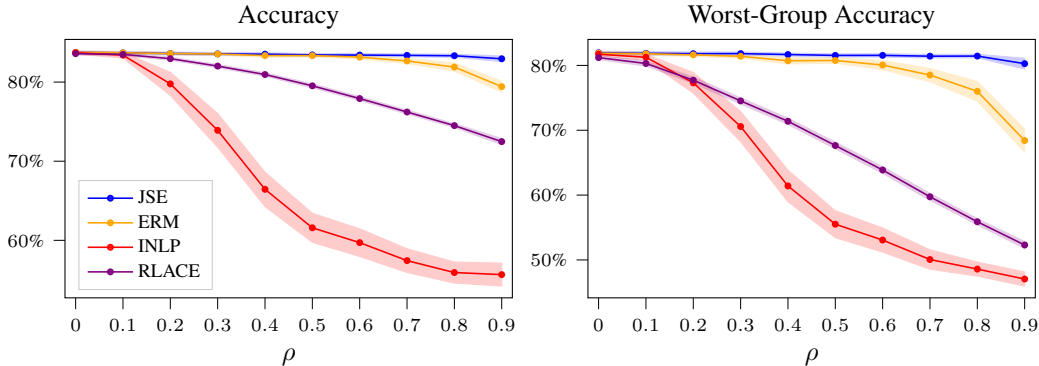


Figure 4: **OOD generalization for the Toy dataset:** We plot the (worst-group) accuracy on an OOD test set without spurious correlation, as a function of the spurious correlation in the training data. Each accuracy is obtained by averaging over 100 runs. The shaded area reflects the 95% confidence interval.

Figure 4 shows the effect of different concept-removal methods to OOD generalization. The concept-removal methods were applied to 2,000 training datapoints with varying correlation ρ , and tested on 2,000 datapoints drawn from a distribution without spurious correlation ($\rho = 0$). For ERM, the average and worst-group accuracy degrade because the trained model increasingly relies on the spurious feature. The loss in performance of INLP and RLACE has a different origin: as the spurious correlation increases, more of the main-task information is removed from the embedding space. The performance of JSE remains constant, with a marginal decrease at $\rho = 0.9$.

4.2 WATERBIRDS & CELEBA

We use two common computer vision datasets containing a spurious correlation. The first is the Waterbirds dataset (Sagawa et al., 2019), where the main-task concept is bird type (waterbird vs. landbird) and the spurious concept is background (water vs. land). The second is the CelebA dataset, where the main-task concept is hair color (blond vs. non-blond) and the spurious concept is sex (female vs. male). We use a pre-trained Resnet50 architecture (He et al., 2016) without finetuning, which is unnecessary for strong performance on either dataset (Izmailov et al., 2022). To increase the precision of our method and computational efficiency, we reduce the dimension of the last-layer embeddings from 2,048 to 100 via Principal Component Analysis (PCA).

For these datasets we cannot directly control the strength of the spurious relation between the main-task label and the spurious features, $p_{\text{train}}(y_{\text{mt}}|\mathbf{z}_{\text{sp}})$. We therefore use $p_{\text{train}}(y_{\text{mt}} = y|y_{\text{sp}} = y)$, with $y \in \{0, 1\}$ as a proxy. Because Waterbirds is a synthetic dataset, we create new versions of the dataset containing 4,795 training images. To train CelebA, we create samples of size 4,500 from the original dataset and in which the main-task label (blond vs. non-blond) is balanced.

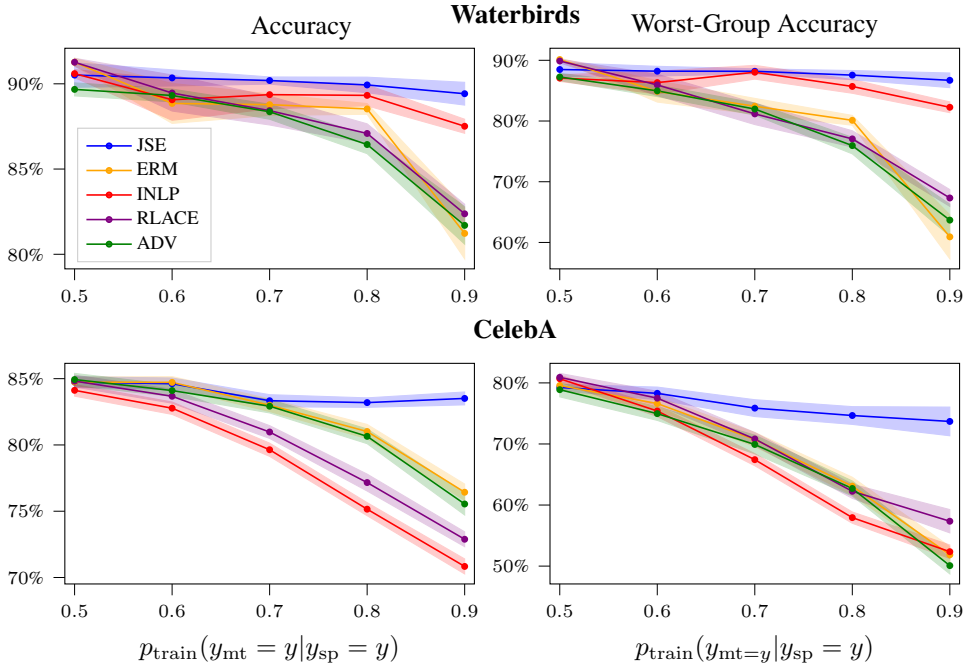


Figure 5: **OOD generalization for the Waterbirds and CelebA datasets:** We plot the (worst-group) accuracy on an OOD test set where $p_{\text{OOD}}(y_{\text{mt}} = y|y_{\text{sp}} = y) = 0.5$, as a function of $p_{\text{train}}(y_{\text{mt}} = y|y_{\text{sp}} = y)$. Each accuracy is obtained by averaging over 20 runs. The shaded area reflects the 95% confidence interval.

Figure 5 shows the results of applying different concept-removal methods. The classifiers are trained on data with varying spurious correlation and tested on OOD data where $p_{\text{OOD}}(y_{\text{mt}}|y_{\text{sp}}) = 0.5$. For both datasets JSE outperforms the other methods, in particular when the spurious correlation is strong. ERM, INLP and RLACE suffer from the same problems as described in Section 4.1. For ADV the performance deteriorates because the spurious features remain present after the training procedure, in line with previous work (Belinkov, 2022; Ravfogel et al., 2022a). Although much smaller, JSE also shows performance loss. As the spurious correlation increases, we suspect our method becomes more sensitive to finite-sample estimation noise. We illustrate this further in Appendix B.2 for the Toy dataset.

From a different perspective, JSE attempts to make a neural network focus on the right (i.e. causally related) features. Figure 6 shows this using Grad-CAM (Selvaraju et al., 2017). Although all trained to predict bird type, only for JSE the classifier relies predominantly on the bird features and neglects the background. Interestingly, both INLP and RLACE perform much worse on images that appear more frequently in the training set (e.g. landbirds on land) than on images from minority groups (e.g. landbirds on water). We posit that this is because features get mixed, as described by Kumar et al. (2022), leading INLP or RLACE to associate spurious features with the main-task concept. This can also be seen in Figure 6, where after INLP a landbird is classified as a waterbird with use of the land background.

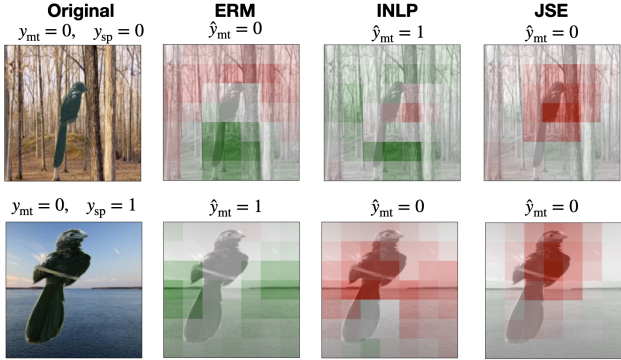


Figure 6: **Grad-CAM for the last layer of Resnet-50 predicting the main-task label:** Red (green) patches indicate a contribution towards the correct (incorrect) predicted class. ERM and INLP use the background for both their correct and incorrect predictions.

4.3 MULTINLI

For an NLP application we use the MultiNLI dataset (Williams et al., 2018), which contains pairs of sentences. The main-task concept is whether or not the first sentence contradicts the second sentence. Following an experiment from Joshi et al. (2022), we use as spurious concept the presence or absence of a punctuation mark (!!) at the end of the second sentence. For exemplary pairs of sentences, see Appendix F. As in the case of the vision experiments, we use $p(y_{\text{mt}} = y | y_{\text{sp}} = y)$ with $y \in \{0, 1\}$ to control the strength of the spurious correlation. Each run in our experiments starts with finetuning a BERT model, after which concept removal is applied to the [CLS] embeddings. The size of the training set is 50,000, and again we use PCA to reduce the dimensionality of the embeddings from 768 to 100.

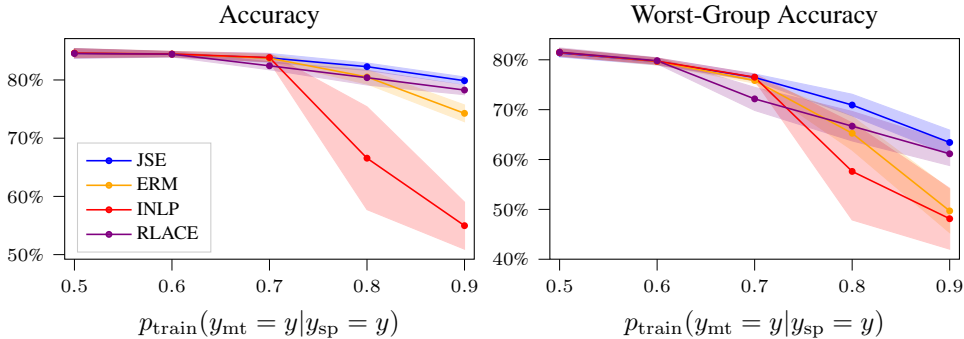


Figure 7: **OOD generalization for MultiNLI dataset:** We plot the (worst-group) accuracy on an OOD test set without spurious correlation ($p_{\text{OOD}}(y_{\text{mt}} = y | y_{\text{sp}} = y) = 0.5$), as a function of $p_{\text{train}}(y_{\text{mt}} = y | y_{\text{sp}} = y)$. Each accuracy is obtained by averaging over 5 runs. The shaded area reflects the 95% confidence interval.

Figure 7 shows the OOD generalization of different concept-removal methods applied to the MultiNLI dataset (analogous to Figure 5 for vision). JSE still outperforms the other concept-removal methods for strong correlations. However, compared to the vision datasets, it exhibits a larger performance loss for increasing spurious correlation. We suspect that during finetuning of BERT the main-task concept and spurious concept become overlapping in the [CLS] embedding, in line with observations from previous work by Dalvi et al. (2022). Notice that the classifier trained after INLP has a performance comparable to a random classifier, in line with what was observed in Kumar et al. (2022). By contrast, the performance of RLACE is close to JSE’s, although it appears to be mixing spurious and main-task features, as it did for the vision datasets. Attempts to perform adversarial removal on this dataset leads to convergence issues, which has been previously noted as a problem for these types of methods (Xing et al., 2021).

5 CONCLUSION AND DISCUSSION

This paper has introduced and empirically tested joint subspace estimation (JSE), a novel post-hoc concept-removal method that addresses OOD generalization due to spurious correlations by identifying two orthogonal linear subspaces associated with the main-task and spurious features.

JSE consistently outperforms existing concept-removal methods, despite making particular assumptions (linearity, orthogonality) about the structure of the embedding space. Future work should consider developing tests for these assumptions, or see whether they can be relaxed. One example is to see if we can jointly estimate subspaces based on their non-linear relationship with the spurious and main-task labels, as done by Ravfogel et al. (2022b) for RLACE.

Our results also highlight the difficulty of separating different concepts in the [CLS] embeddings of BERT. All post-hoc concept-removal methods we consider perform relatively better for the vision datasets than the MultiNLI dataset. This highlights the need to better disentangle concepts in embeddings of large language models, for instance through different training procedures, similar to the work of Zhang et al. (2021).

REFERENCES

- Kartik Ahuja, Ethan Caballero, Dinghuai Zhang, Jean-Christophe Gagnon-Audet, Yoshua Bengio, Ioannis Mitliagkas, and Irina Rish. Invariance principle meets information bottleneck for out-of-distribution generalization. In M. Ranzato, A. Beygelzimer, Y. Dauphin, P.S. Liang, and J. Wortman Vaughan (eds.), *Advances in Neural Information Processing Systems*, volume 34, pp. 3438–3450, 2021. URL https://proceedings.neurips.cc/paper_files/paper/2021/file/1c336b8080f82bcc2cd2499b4c57261d-Paper.pdf.
- Guillaume Alain and Yoshua Bengio. Understanding intermediate layers using linear classifier probes. In *5th International Conference on Learning Representations, ICLR 2017, Toulon, France, April 24-26, 2017, Workshop Track Proceedings*. OpenReview.net, 2017. URL <https://openreview.net/forum?id=HJ4-rAVt1>.
- Martín Arjovsky, Léon Bottou, Ishaan Gulrajani, and David Lopez-Paz. Invariant risk minimization. *CoRR*, abs/1907.02893, 2019. URL <https://arxiv.org/abs/1907.02893>.
- David Bau, Bolei Zhou, Aditya Khosla, Aude Oliva, and Antonio Torralba. Network dissection: Quantifying interpretability of deep visual representations. In *2017 IEEE Conference on Computer Vision and Pattern Recognition (CVPR)*, pp. 3319–3327, 2017. doi: 10.1109/CVPR.2017.354.
- Yonatan Belinkov. Probing classifiers: Promises, shortcomings, and advances. *Computational Linguistics*, 48(1):207–219, March 2022. doi: 10.1162/coli.a.00422. URL <https://aclanthology.org/2022.cl-1.7>.
- Tolga Bolukbasi, Kai-Wei Chang, James Y Zou, Venkatesh Saligrama, and Adam T Kalai. Man is to computer programmer as woman is to homemaker? debiasing word embeddings. In D. Lee, M. Sugiyama, U. Luxburg, I. Guyon, and R. Garnett (eds.), *Advances in Neural Information Processing Systems*, volume 29. Curran Associates, Inc., 2016. URL https://proceedings.neurips.cc/paper_files/paper/2016/file/a486cd07e4ac3d270571622f4f316ec5-Paper.pdf.
- Zhi Chen, Yijie Bei, and Cynthia Rudin. Concept whitening for interpretable image recognition. *Nature Machine Intelligence*, 2(12):772–782, 2020. doi: 10.1038/s42256-020-00265-z. URL <https://doi.org/10.1038/s42256-020-00265-z>.
- Fahim Dalvi, Abdul Rafae Khan, Firoj Alam, Nadir Durrani, Jia Xu, and Hassan Sajjad. Discovering latent concepts learned in BERT. In *The Tenth International Conference on Learning Representations, ICLR 2022, Virtual Event, April 25-29, 2022*. OpenReview.net, 2022. URL <https://openreview.net/forum?id=POTMtpYI1xH>.
- Alexander D’Amour, Katherine A. Heller, Dan Moldovan, Ben Adlam, Babak Alipanahi, Alex Beutel, Christina Chen, Jonathan Deaton, Jacob Eisenstein, Matthew D. Hoffman, Farhad Hormozdiari, Neil Houlsby, Shaobo Hou, Ghassen Jerfel, Alan Karthikesalingam, Mario Lucic, Yi-An Ma, Cory Y. McLean, Diana Mincu, Akinori Mitani, Andrea Montanari, Zachary Nado, Vivek Natarajan, Christopher Nielson, Thomas F. Osborne, Rajiv Raman, Kim Ramasamy, Rory Sayres, Jessica Schrouff, Martin Seneviratne, Shannon Sequeira, Harini Suresh, Victor Veitch, Max Vladymyrov, Xuezhong Wang, Kellie Webster, Steve Yadlowsky, Taedong Yun, Xiaohua Zhai, and D. Sculley. Underspecification presents challenges for credibility in modern machine learning. *Arxiv Computing Research Repository (CoRR)*, abs/2011.03395, 2020. URL <https://arxiv.org/abs/2011.03395>.
- Sunipa Dev and Jeff Phillips. Attenuating bias in word vectors. In Kamalika Chaudhuri and Masashi Sugiyama (eds.), *Proceedings of the Twenty-Second International Conference on Artificial Intelligence and Statistics*, volume 89 of *Proceedings of Machine Learning Research*, pp. 879–887. PMLR, 16–18 Apr 2019. URL <https://proceedings.mlr.press/v89/dev19a.html>.
- Sunipa Dev, Tao Li, Jeff M Phillips, and Vivek Srikumar. OSCaR: Orthogonal subspace correction and rectification of biases in word embeddings. In *Proceedings of the 2021 Conference on Empirical Methods in Natural Language Processing*, pp. 5034–5050, Online and Punta Cana, Dominican

- Republic, November 2021. Association for Computational Linguistics. doi: 10.18653/v1/2021.emnlp-main.411. URL <https://aclanthology.org/2021.emnlp-main.411>.
- Jacob Devlin, Ming-Wei Chang, Kenton Lee, and Kristina Toutanova. BERT: pre-training of deep bidirectional transformers for language understanding. *CoRR*, abs/1810.04805, 2018. URL <http://arxiv.org/abs/1810.04805>.
- Harrison Edwards and Amos Storkey. Censoring representations with an adversary. In *International Conference in Learning Representations (ICLR2016)*, pp. 1–14, May 2016. URL <https://iclr.cc/archive/www/doku.php%3Fid=iclr2016:main.html>. 4th International Conference on Learning Representations, ICLR 2016 ; Conference date: 02-05-2016 Through 04-05-2016.
- Yanai Elazar and Yoav Goldberg. Adversarial removal of demographic attributes from text data. In *Proceedings of the 2018 Conference on Empirical Methods in Natural Language Processing*, pp. 11–21, Brussels, Belgium, October-November 2018. Association for Computational Linguistics. doi: 10.18653/v1/D18-1002. URL <https://aclanthology.org/D18-1002>.
- Kawin Ethayarajh, David Duvenaud, and Graeme Hirst. Understanding undesirable word embedding associations. In *Proceedings of the 57th Annual Meeting of the Association for Computational Linguistics*, pp. 1696–1705, Florence, Italy, July 2019. Association for Computational Linguistics. doi: 10.18653/v1/P19-1166. URL <https://aclanthology.org/P19-1166>.
- Yaroslav Ganin and Victor Lempitsky. Unsupervised domain adaptation by backpropagation. In Francis Bach and David Blei (eds.), *Proceedings of the 32nd International Conference on Machine Learning*, volume 37 of *Proceedings of Machine Learning Research*, pp. 1180–1189, Lille, France, 07–09 Jul 2015. PMLR. URL <https://proceedings.mlr.press/v37/ganin15.html>.
- Robert Geirhos, Patricia Rubisch, Claudio Michaelis, Matthias Bethge, Felix A. Wichmann, and Wieland Brendel. Imagenet-trained CNNs are biased towards texture; increasing shape bias improves accuracy and robustness. In *International Conference on Learning Representations*, 2019. URL <https://openreview.net/forum?id=Bygh9j09KX>.
- Robert Geirhos, Jörn-Henrik Jacobsen, Claudio Michaelis, Richard S. Zemel, Wieland Brendel, Matthias Bethge, and Felix A. Wichmann. Shortcut learning in deep neural networks. *Arxiv Computing Research Repository (CoRR)*, abs/2004.07780, 2020. URL <https://arxiv.org/abs/2004.07780>.
- Ian Goodfellow, Jean Pouget-Abadie, Mehdi Mirza, Bing Xu, David Warde-Farley, Sherjil Ozair, Aaron Courville, and Yoshua Bengio. Generative adversarial nets. In Z. Ghahramani, M. Welling, C. Cortes, N. Lawrence, and K.Q. Weinberger (eds.), *Advances in Neural Information Processing Systems*, volume 27. Curran Associates, Inc., 2014. URL https://proceedings.neurips.cc/paper_files/paper/2014/file/5ca3e9b122f61f8f06494c97b1afccf3-Paper.pdf.
- Suchin Gururangan, Swabha Swayamdipta, Omer Levy, Roy Schwartz, Samuel Bowman, and Noah A. Smith. Annotation artifacts in natural language inference data. In *Proceedings of the 2018 Conference of the North American Chapter of the Association for Computational Linguistics: Human Language Technologies, Volume 2 (Short Papers)*, pp. 107–112, New Orleans, Louisiana, June 2018. Association for Computational Linguistics. doi: 10.18653/v1/N18-2017. URL <https://aclanthology.org/N18-2017>.
- Kaiming He, Xiangyu Zhang, Shaoqing Ren, and Jian Sun. Deep residual learning for image recognition. In *Proceedings of the IEEE Conference on Computer Vision and Pattern Recognition (CVPR)*, June 2016.
- Katherine Hermann, Ting Chen, and Simon Kornblith. The origins and prevalence of texture bias in convolutional neural networks. In H. Larochelle, M. Ranzato, R. Hadsell, M.F. Balcan, and H. Lin (eds.), *Advances in Neural Information Processing Systems*, volume 33, pp. 19000–19015. Curran Associates, Inc., 2020. URL https://proceedings.neurips.cc/paper_files/paper/2020/file/db5f9f42a7157abe65bb145000b5871a-Paper.pdf.

- Badr Youbi Idrissi, Martin Arjovsky, Mohammad Pezeshki, and David Lopez-Paz. Simple data balancing achieves competitive worst-group-accuracy. In *First Conference on Causal Learning and Reasoning*, 2022. URL <https://openreview.net/forum?id=cDxT7WYhaD>.
- Pavel Izmailov, Polina Kirichenko, Nate Gruver, and Andrew G Wilson. On feature learning in the presence of spurious correlations. In S. Koyejo, S. Mohamed, A. Agarwal, D. Belgrave, K. Cho, and A. Oh (eds.), *Advances in Neural Information Processing Systems*, volume 35, pp. 38516–38532. Curran Associates, Inc., 2022. URL https://proceedings.neurips.cc/paper_files/paper/2022/file/fb64a552feda3d981dbe43527a80a07e-Paper-Conference.pdf.
- Nitish Joshi, Xiang Pan, and He He. Are all spurious features in natural language alike? an analysis through a causal lens. In *Proceedings of the 2022 Conference on Empirical Methods in Natural Language Processing*, pp. 9804–9817, Abu Dhabi, United Arab Emirates, December 2022. Association for Computational Linguistics. doi: 10.18653/v1/2022.emnlp-main.666. URL <https://aclanthology.org/2022.emnlp-main.666>.
- Divyansh Kaushik and Zachary C. Lipton. How much reading does reading comprehension require? a critical investigation of popular benchmarks. In *Proceedings of the 2018 Conference on Empirical Methods in Natural Language Processing*, pp. 5010–5015, Brussels, Belgium, October–November 2018. Association for Computational Linguistics. doi: 10.18653/v1/D18-1546. URL <https://aclanthology.org/D18-1546>.
- Been Kim, Martin Wattenberg, Justin Gilmer, Carrie Cai, James Wexler, Fernanda Viegas, and Rory sayres. Interpretability beyond feature attribution: Quantitative testing with concept activation vectors (TCAV). In Jennifer Dy and Andreas Krause (eds.), *Proceedings of the 35th International Conference on Machine Learning*, volume 80 of *Proceedings of Machine Learning Research*, pp. 2668–2677. PMLR, 10–15 Jul 2018. URL <https://proceedings.mlr.press/v80/kim18d.html>.
- Diederik P. Kingma and Jimmy Ba. Adam: A method for stochastic optimization. In Yoshua Bengio and Yann LeCun (eds.), *3rd International Conference on Learning Representations, ICLR 2015, San Diego, CA, USA, May 7-9, 2015, Conference Track Proceedings*, 2015. URL <http://arxiv.org/abs/1412.6980>.
- Polina Kirichenko, Pavel Izmailov, and Andrew Gordon Wilson. Last layer re-training is sufficient for robustness to spurious correlations. In *The Eleventh International Conference on Learning Representations, ICLR 2023, Kigali, Rwanda, May 1-5, 2023*. OpenReview.net, 2023. URL <https://openreview.net/pdf?id=Zb6c8A-Fghk>.
- Abhinav Kumar, Chenhao Tan, and Amit Sharma. Probing classifiers are unreliable for concept removal and detection. In S. Koyejo, S. Mohamed, A. Agarwal, D. Belgrave, K. Cho, and A. Oh (eds.), *Advances in Neural Information Processing Systems*, volume 35, pp. 17994–18008. Curran Associates, Inc., 2022. URL https://proceedings.neurips.cc/paper_files/paper/2022/file/725f5e8036cc08adeba4a7c3bcbc6f2c-Paper-Conference.pdf.
- Ziwei Liu, Ping Luo, Xiaogang Wang, and Xiaoou Tang. Deep learning face attributes in the wild. In *Proceedings of International Conference on Computer Vision (ICCV)*, December 2015.
- Tom McCoy, Ellie Pavlick, and Tal Linzen. Right for the wrong reasons: Diagnosing syntactic heuristics in natural language inference. In *Proceedings of the 57th Annual Meeting of the Association for Computational Linguistics*, pp. 3428–3448, Florence, Italy, July 2019. Association for Computational Linguistics. doi: 10.18653/v1/P19-1334. URL <https://aclanthology.org/P19-1334>.
- Timothy Niven and Hung-Yu Kao. Probing neural network comprehension of natural language arguments. In *Proceedings of the 57th Annual Meeting of the Association for Computational Linguistics*, pp. 4658–4664, Florence, Italy, July 2019. Association for Computational Linguistics. doi: 10.18653/v1/P19-1459. URL <https://aclanthology.org/P19-1459>.

- Mohammad Pezeshki, Oumar Kaba, Yoshua Bengio, Aaron C Courville, Doina Precup, and Guillaume Lajoie. Gradient starvation: A learning proclivity in neural networks. In M. Ranzato, A. Beygelzimer, Y. Dauphin, P.S. Liang, and J. Wortman Vaughan (eds.), *Advances in Neural Information Processing Systems*, volume 34, pp. 1256–1272. Curran Associates, Inc., 2021. URL https://proceedings.neurips.cc/paper_files/paper/2021/file/0987b8b338d6c90bbedd8631bc499221-Paper.pdf.
- Aahlad Manas Puli, Lily H. Zhang, Eric Karl Oermann, and Rajesh Ranganath. Out-of-distribution generalization in the presence of nuisance-induced spurious correlations. In *The Tenth International Conference on Learning Representations, ICLR 2022, Virtual Event, April 25-29, 2022*. OpenReview.net, 2022. URL <https://openreview.net/forum?id=12RoR2o32T>.
- Nasim Rahaman, Aristide Baratin, Devansh Arpit, Felix Draxler, Min Lin, Fred Hamprecht, Yoshua Bengio, and Aaron Courville. On the spectral bias of neural networks. In Kamalika Chaudhuri and Ruslan Salakhutdinov (eds.), *Proceedings of the 36th International Conference on Machine Learning*, volume 97 of *Proceedings of Machine Learning Research*, pp. 5301–5310. PMLR, 09–15 Jun 2019. URL <https://proceedings.mlr.press/v97/rahaman19a.html>.
- Shauli Ravfogel, Yanai Elazar, Hila Gonen, Michael Twiton, and Yoav Goldberg. Null it out: Guarding protected attributes by iterative nullspace projection. In *Proceedings of the 58th Annual Meeting of the Association for Computational Linguistics*, pp. 7237–7256, Online, July 2020. Association for Computational Linguistics. doi: 10.18653/v1/2020.acl-main.647. URL <https://aclanthology.org/2020.acl-main.647>.
- Shauli Ravfogel, Michael Twiton, Yoav Goldberg, and Ryan D Cotterell. Linear adversarial concept erasure. In Kamalika Chaudhuri, Stefanie Jegelka, Le Song, Csaba Szepesvari, Gang Niu, and Sivan Sabato (eds.), *Proceedings of the 39th International Conference on Machine Learning*, volume 162 of *Proceedings of Machine Learning Research*, pp. 18400–18421. PMLR, 17–23 Jul 2022a. URL <https://proceedings.mlr.press/v162/ravfogel22a.html>.
- Shauli Ravfogel, Francisco Vargas, Yoav Goldberg, and Ryan Cotterell. Adversarial concept erasure in kernel space. In *Proceedings of the 2022 Conference on Empirical Methods in Natural Language Processing*, pp. 6034–6055, Abu Dhabi, United Arab Emirates, December 2022b. Association for Computational Linguistics. URL <https://aclanthology.org/2022.emnlp-main.405>.
- Shauli Ravfogel, Yoav Goldberg, and Ryan Cotterell. Log-linear guardedness and its implications. In *Proceedings of the 61st Annual Meeting of the Association for Computational Linguistics (Volume 1: Long Papers)*, pp. 9413–9431, Toronto, Canada, July 2023. Association for Computational Linguistics. doi: 10.18653/v1/2023.acl-long.523. URL <https://aclanthology.org/2023.acl-long.523>.
- A Rényi. On the asymptotic distribution of the sum of a random number of independent random variables. *Acta Math*, 8:193–199, 1957.
- Elan Rosenfeld, Pradeep Kumar Ravikumar, and Andrej Risteski. Domain-adjusted regression or: ERM may already learn features sufficient for out-of-distribution generalization. In *NeurIPS 2022 Workshop on Distribution Shifts: Connecting Methods and Applications*, 2022. URL <https://openreview.net/forum?id=Ypo0AckYW8>.
- Shiori Sagawa, Pang Wei Koh, Tatsunori B. Hashimoto, and Percy Liang. Distributionally robust neural networks for group shifts: On the importance of regularization for worst-case generalization. *Arxiv Computing Research Repository (CoRR)*, abs/1911.08731, 2019. URL <http://arxiv.org/abs/1911.08731>.
- Shiori Sagawa, Aditi Raghunathan, Pang Wei Koh, and Percy Liang. An investigation of why overparameterization exacerbates spurious correlations. *Arxiv Computing Research Repository (CoRR)*, abs/2005.04345, 2020. URL <https://arxiv.org/abs/2005.04345>.
- Ramprasaath R. Selvaraju, Michael Cogswell, Abhishek Das, Ramakrishna Vedantam, Devi Parikh, and Dhruv Batra. Grad-cam: Visual explanations from deep networks via gradient-based localization. In *2017 IEEE International Conference on Computer Vision (ICCV)*, pp. 618–626, 2017. doi: 10.1109/ICCV.2017.74.

- Sahil Singla and Soheil Feizi. Salient imagenet: How to discover spurious features in deep learning? In *International Conference on Learning Representations*, 2022. URL <https://openreview.net/forum?id=XVPqLyNxSyh>.
- Megha Srivastava, Tatsunori Hashimoto, and Percy Liang. Robustness to spurious correlations via human annotations. In Hal Daumé III and Aarti Singh (eds.), *Proceedings of the 37th International Conference on Machine Learning*, volume 119 of *Proceedings of Machine Learning Research*, pp. 9109–9119. PMLR, 13–18 Jul 2020. URL <https://proceedings.mlr.press/v119/srivastava20a.html>.
- Francisco Vargas and Ryan Cotterell. Exploring the linear subspace hypothesis in gender bias mitigation. In *Proceedings of the 2020 Conference on Empirical Methods in Natural Language Processing (EMNLP)*, pp. 2902–2913, Online, November 2020. Association for Computational Linguistics. doi: 10.18653/v1/2020.emnlp-main.232. URL <https://aclanthology.org/2020.emnlp-main.232>.
- Liwen Wang, Yuanmeng Yan, Keqing He, Yanan Wu, and Weiran Xu. Dynamically disentangling social bias from task-oriented representations with adversarial attack. In *Proceedings of the 2021 Conference of the North American Chapter of the Association for Computational Linguistics: Human Language Technologies*, pp. 3740–3750, Online, June 2021. Association for Computational Linguistics. doi: 10.18653/v1/2021.naacl-main.293. URL <https://aclanthology.org/2021.naacl-main.293>.
- Zhao Wang and Aron Culotta. Identifying spurious correlations for robust text classification. In *Findings of the Association for Computational Linguistics: EMNLP 2020*, pp. 3431–3440, Online, November 2020. Association for Computational Linguistics. doi: 10.18653/v1/2020.findings-emnlp.308. URL <https://aclanthology.org/2020.findings-emnlp.308>.
- Peter Welinder, Steve Branson, Takeshi Mita, Catherine Wah, Florian Schroff, Serge Belongie, and Pietro Perona. Caltech-ucsd birds 200. Technical Report CNS-TR-201, Caltech, 2010. URL <http://www.vision.caltech.edu/visipedia/CUB-200.html>.
- Adina Williams, Nikita Nangia, and Samuel Bowman. A broad-coverage challenge corpus for sentence understanding through inference. In *Proceedings of the 2018 Conference of the North American Chapter of the Association for Computational Linguistics: Human Language Technologies, Volume 1 (Long Papers)*, pp. 1112–1122. Association for Computational Linguistics, 2018. URL <http://aclweb.org/anthology/N18-1101>.
- Thomas Wolf, Lysandre Debut, Victor Sanh, Julien Chaumond, Clement Delangue, Anthony Moi, Pierric Cistac, Tim Rault, Rémi Louf, Morgan Funtowicz, and Jamie Brew. Huggingface’s transformers: State-of-the-art natural language processing. *CoRR*, abs/1910.03771, 2019. URL <http://arxiv.org/abs/1910.03771>.
- Kai Yuanqing Xiao, Logan Engstrom, Andrew Ilyas, and Aleksander Madry. Noise or signal: The role of image backgrounds in object recognition. In *9th International Conference on Learning Representations, ICLR 2021, Virtual Event, Austria, May 3-7, 2021*. OpenReview.net, 2021. URL <https://openreview.net/forum?id=g13D-xY7wLq>.
- Yue Xing, Qifan Song, and Guang Cheng. On the algorithmic stability of adversarial training. In M. Ranzato, A. Beygelzimer, Y. Dauphin, P.S. Liang, and J. Wortman Vaughan (eds.), *Advances in Neural Information Processing Systems*, volume 34, pp. 26523–26535. Curran Associates, Inc., 2021. URL https://proceedings.neurips.cc/paper_files/paper/2021/file/df1f1d20ee86704251795841e6a9405a-Paper.pdf.
- Brian Hu Zhang, Blake Lemoine, and Margaret Mitchell. Mitigating unwanted biases with adversarial learning. In *Proceedings of the 2018 AAAI/ACM Conference on AI, Ethics, and Society*, AIES ’18, pp. 335–340, New York, NY, USA, 2018. Association for Computing Machinery. ISBN 9781450360128. doi: 10.1145/3278721.3278779. URL <https://doi.org/10.1145/3278721.3278779>.

Xiongyi Zhang, Jan-Willem van de Meent, and Byron Wallace. Disentangling representations of text by masking transformers. In *Proceedings of the 2021 Conference on Empirical Methods in Natural Language Processing*, pp. 778–791, Online and Punta Cana, Dominican Republic, November 2021. Association for Computational Linguistics. doi: 10.18653/v1/2021.emnlp-main.60. URL <https://aclanthology.org/2021.emnlp-main.60>.

Bolei Zhou, Aditya Khosla, Àgata Lapedriza, Antonio Torralba, and Aude Oliva. Places: An image database for deep scene understanding. *Arxiv Computing Research Repository (CoRR)*, abs/1610.02055, 2016. URL <http://arxiv.org/abs/1610.02055>.

Chunting Zhou, Xuezhe Ma, Paul Michel, and Graham Neubig. Examining and combating spurious features under distribution shift. In Marina Meila and Tong Zhang (eds.), *Proceedings of the 38th International Conference on Machine Learning*, volume 139 of *Proceedings of Machine Learning Research*, pp. 12857–12867. PMLR, 18–24 Jul 2021. URL <https://proceedings.mlr.press/v139/zhou21g.html>.

APPENDIX OUTLINE

This appendix is organized as follows. In Section A, we give more details on the results for the four datasets (Waterbirds, CelebA, MultiNLI and Toy) used in the experiments. Section B contains several additional results for the Toy dataset. In Section C we present additional details on the implementation of the JSE algorithm. In Section D we lay out the testing procedure for the JSE algorithm. In Section E, we compare JSE to group-weighted ERM. Finally, Section F provides a more detailed description of the datasets, as well as implementation details for the experiments.

A FULL SET OF RESULTS FOR WATERBIRDS, CELEBA, MULTINLI AND TOY DATASET

Method	Accuracy	$p_{\text{train}}(y_{\text{mt}} = y y_{\text{sp}} = y)$				
		0.5	0.6	0.7	0.8	0.9
JSE	$y_{\text{mt}} = 0, y_{\text{sp}} = 0$	91.88 (0.45)	91.65 (0.30)	91.20 (0.16)	91.13 (0.41)	90.23 (0.79)
	$y_{\text{mt}} = 0, y_{\text{sp}} = 1$	88.59 (0.60)	88.22 (0.41)	88.19 (0.21)	87.56 (0.39)	87.34 (0.49)
	$y_{\text{mt}} = 1, y_{\text{sp}} = 0$	90.98 (0.22)	91.35 (0.18)	91.81 (0.10)	91.64 (0.24)	91.81 (0.24)
	$y_{\text{mt}} = 1, y_{\text{sp}} = 1$	91.99 (0.18)	92.28 (0.14)	92.06 (0.13)	92.38 (0.19)	91.48 (0.22)
	Worst-group	88.48 (0.58)	88.21 (0.41)	88.19 (0.21)	87.56 (0.39)	86.70 (0.62)
	Average	90.51 (0.37)	90.35 (0.24)	90.19 (0.11)	89.93 (0.23)	89.42 (0.34)
ERM	$y_{\text{mt}} = 0, y_{\text{sp}} = 0$	91.70 (0.19)	90.88 (0.82)	93.14 (0.29)	95.27 (0.06)	96.17 (0.25)
	$y_{\text{mt}} = 0, y_{\text{sp}} = 1$	91.10 (0.20)	84.87 (0.90)	82.43 (0.66)	80.12 (0.41)	60.92 (1.85)
	$y_{\text{mt}} = 1, y_{\text{sp}} = 0$	91.18 (0.15)	91.32 (0.36)	90.49 (0.21)	88.32 (0.11)	84.72 (0.43)
	$y_{\text{mt}} = 1, y_{\text{sp}} = 1$	90.40 (0.14)	93.22 (0.18)	94.03 (0.15)	94.59 (0.09)	96.56 (0.16)
	Worst-group	90.13 (0.10)	84.87 (0.90)	82.43 (0.66)	80.12 (0.41)	60.92 (1.85)
	Average	91.27 (0.11)	88.85 (0.60)	88.78 (0.32)	88.53 (0.16)	81.23 (0.76)
INLP	$y_{\text{mt}} = 0, y_{\text{sp}} = 0$	93.89 (0.13)	90.13 (0.78)	88.76 (0.61)	85.70 (0.58)	82.38 (0.50)
	$y_{\text{mt}} = 0, y_{\text{sp}} = 1$	87.14 (0.30)	86.35 (0.97)	88.54 (0.63)	91.90 (0.36)	91.83 (0.24)
	$y_{\text{mt}} = 1, y_{\text{sp}} = 0$	89.41 (0.20)	91.71 (0.30)	92.64 (0.17)	93.23 (0.21)	92.73 (0.26)
	$y_{\text{mt}} = 1, y_{\text{sp}} = 1$	92.38 (0.13)	92.21 (0.26)	91.08 (0.29)	89.08 (0.26)	85.13 (0.37)
	Worst-group	87.07 (0.28)	86.33 (0.96)	88.04 (0.58)	85.70 (0.58)	82.26 (0.45)
	Average	90.60 (0.12)	89.07 (0.62)	89.36 (0.42)	89.32 (0.31)	87.51 (0.21)
RLACE	$y_{\text{mt}} = 0, y_{\text{sp}} = 0$	92.21 (0.19)	86.27 (0.96)	81.18 (0.90)	77.06 (0.69)	68.14 (0.77)
	$y_{\text{mt}} = 0, y_{\text{sp}} = 1$	90.57 (0.25)	91.44 (0.60)	94.26 (0.36)	96.27 (0.13)	96.45 (0.12)
	$y_{\text{mt}} = 1, y_{\text{sp}} = 0$	90.83 (0.16)	93.64 (0.22)	94.89 (0.15)	95.40 (0.17)	95.26 (0.17)
	$y_{\text{mt}} = 1, y_{\text{sp}} = 1$	90.85 (0.19)	89.52 (0.35)	86.95 (0.33)	81.78 (0.37)	70.06 (0.61)
	Worst-group	89.88 (0.15)	85.94 (0.89)	81.18 (0.90)	77.06 (0.69)	67.33 (0.71)
	Average	91.27 (0.12)	89.46 (0.54)	88.43 (0.43)	87.09 (0.29)	82.37 (0.29)
ADV	$y_{\text{mt}} = 0, y_{\text{sp}} = 0$	91.66 (0.25)	93.54 (0.34)	94.50 (0.33)	96.41 (0.19)	97.19 (0.21)
	$y_{\text{mt}} = 0, y_{\text{sp}} = 1$	90.71 (0.30)	86.00 (0.61)	82.41 (0.60)	76.52 (0.81)	64.04 (1.47)
	$y_{\text{mt}} = 1, y_{\text{sp}} = 0$	88.77 (0.38)	87.23 (0.48)	84.59 (0.58)	79.91 (0.64)	70.76 (1.21)
	$y_{\text{mt}} = 1, y_{\text{sp}} = 1$	87.57 (0.33)	90.37 (0.29)	91.74 (0.26)	92.53 (0.27)	94.05 (0.22)
	Worst-group	87.25 (0.31)	84.97 (0.48)	81.97 (0.51)	75.95 (0.69)	63.68 (1.34)
	Average	89.67 (0.20)	89.32 (0.19)	88.36 (0.22)	86.44 (0.27)	81.70 (0.56)

Table 1: **Results for the Waterbirds dataset:** Table shows the average, worst-group, and per-group accuracy on a test set where $p_{\text{OOD}}(y_{\text{mt}} = y | y_{\text{sp}} = y) = 0.5$, with $y \in \{0, 1\}$, as a function of $p_{\text{train}}(y_{\text{mt}} = y | y_{\text{sp}} = y)$. Each accuracy is obtained by averaging over 20 runs. Standard error is reported between brackets.

Method	Accuracy	$p_{\text{train}}(y_{\text{mt}} = y y_{\text{sp}} = y)$				
		0.5	0.6	0.7	0.8	0.9
JSE	$y_{\text{mt}} = 0, y_{\text{sp}} = 0$	85.83 (0.37)	87.17 (0.33)	87.32 (0.59)	88.32 (0.49)	89.41 (0.60)
	$y_{\text{mt}} = 0, y_{\text{sp}} = 1$	79.36 (0.27)	79.15 (0.29)	78.03 (0.59)	77.48 (0.52)	78.86 (0.66)
	$y_{\text{mt}} = 1, y_{\text{sp}} = 0$	81.94 (0.53)	80.35 (0.79)	76.48 (0.81)	75.27 (0.85)	73.81 (1.22)
	$y_{\text{mt}} = 1, y_{\text{sp}} = 1$	91.84 (0.33)	91.80 (0.38)	91.51 (0.49)	91.71 (0.55)	91.96 (0.44)
	Worst-group	79.25 (0.27)	78.29 (0.52)	75.87 (0.70)	74.66 (0.74)	73.69 (1.20)
	Average	84.74 (0.20)	84.62 (0.22)	83.33 (0.23)	83.19 (0.18)	83.51 (0.25)
ERM	$y_{\text{mt}} = 0, y_{\text{sp}} = 0$	85.16 (0.52)	89.46 (0.41)	91.92 (0.28)	94.24 (0.18)	95.92 (0.23)
	$y_{\text{mt}} = 0, y_{\text{sp}} = 1$	79.79 (0.38)	77.60 (0.36)	74.36 (0.56)	70.60 (0.63)	61.10 (0.85)
	$y_{\text{mt}} = 1, y_{\text{sp}} = 0$	82.30 (0.59)	78.23 (0.76)	71.11 (0.67)	63.10 (0.74)	51.85 (0.69)
	$y_{\text{mt}} = 1, y_{\text{sp}} = 1$	91.72 (0.40)	93.59 (0.27)	94.61 (0.29)	96.11 (0.19)	96.86 (0.12)
	Worst-group	79.57 (0.34)	76.62 (0.54)	70.73 (0.59)	63.10 (0.74)	51.85 (0.69)
	Average	84.74 (0.19)	84.72 (0.22)	83.00 (0.24)	81.01 (0.27)	76.43 (0.31)
INLP	$y_{\text{mt}} = 0, y_{\text{sp}} = 0$	81.44 (0.40)	75.40 (0.46)	67.43 (0.51)	57.94 (0.47)	52.55 (0.60)
	$y_{\text{mt}} = 0, y_{\text{sp}} = 1$	81.40 (0.26)	84.78 (0.23)	86.64 (0.49)	87.39 (0.41)	87.49 (0.35)
	$y_{\text{mt}} = 1, y_{\text{sp}} = 0$	84.78 (0.56)	88.04 (0.48)	89.27 (0.47)	88.09 (0.46)	84.94 (0.65)
	$y_{\text{mt}} = 1, y_{\text{sp}} = 1$	88.86 (0.35)	82.87 (0.57)	75.21 (0.49)	67.20 (0.58)	58.36 (0.57)
	Worst-group	80.68 (0.28)	75.40 (0.46)	67.43 (0.51)	57.94 (0.47)	52.36 (0.57)
	Average	84.12 (0.22)	82.77 (0.24)	79.64 (0.25)	75.16 (0.25)	70.84 (0.29)
RLACE	$y_{\text{mt}} = 0, y_{\text{sp}} = 0$	83.14 (0.46)	77.50 (0.57)	70.82 (0.54)	62.25 (0.59)	57.63 (0.96)
	$y_{\text{mt}} = 0, y_{\text{sp}} = 1$	81.10 (0.36)	84.29 (0.27)	86.44 (0.39)	86.88 (0.35)	85.87 (0.56)
	$y_{\text{mt}} = 1, y_{\text{sp}} = 0$	84.64 (0.49)	88.46 (0.54)	89.96 (0.46)	90.29 (0.43)	85.10 (1.03)
	$y_{\text{mt}} = 1, y_{\text{sp}} = 1$	90.39 (0.42)	84.44 (0.55)	76.68 (0.50)	69.23 (0.76)	62.94 (1.04)
	Worst-group	80.91 (0.33)	77.50 (0.57)	70.82 (0.54)	62.25 (0.59)	57.35 (0.97)
	Average	84.82 (0.23)	83.67 (0.27)	80.97 (0.25)	77.16 (0.33)	72.88 (0.29)
ADV	$y_{\text{mt}} = 0, y_{\text{sp}} = 0$	86.31 (0.38)	89.47 (0.30)	92.17 (0.34)	93.64 (0.28)	95.91 (0.18)
	$y_{\text{mt}} = 0, y_{\text{sp}} = 1$	80.49 (0.42)	77.79 (0.45)	74.47 (0.57)	70.04 (0.68)	59.17 (1.10)
	$y_{\text{mt}} = 1, y_{\text{sp}} = 0$	81.08 (0.91)	75.28 (0.61)	69.97 (0.80)	62.71 (0.63)	50.26 (0.71)
	$y_{\text{mt}} = 1, y_{\text{sp}} = 1$	91.86 (0.36)	93.87 (0.36)	95.08 (0.26)	96.21 (0.21)	96.84 (0.23)
	Worst-group	78.89 (0.60)	74.97 (0.57)	69.92 (0.78)	62.71 (0.63)	50.08 (0.69)
	Average	84.93 (0.24)	84.10 (0.22)	82.92 (0.26)	80.65 (0.28)	75.55 (0.42)

Table 2: **Results for the celebA dataset:** Table shows the average, worst-group, and per-group accuracy on a test set where $p_{\text{OOD}}(y_{\text{mt}} = y | y_{\text{sp}} = y) = 0.5$, with $y \in \{0, 1\}$, as a function of $p_{\text{train}}(y_{\text{mt}} = y | y_{\text{sp}} = y)$. Each accuracy is obtained by averaging over 20 runs. Standard error is reported between brackets.

Method	Accuracy	$p_{\text{train}}(y_{\text{mt}} = y y_{\text{sp}} = y)$				
		0.5	0.6	0.7	0.8	0.9
JSE	$y_{\text{mt}} = 0, y_{\text{sp}} = 0$	87.49 (0.69)	88.83 (0.52)	90.34 (0.36)	92.53 (0.47)	93.94 (0.56)
	$y_{\text{mt}} = 0, y_{\text{sp}} = 1$	87.31 (0.42)	84.30 (0.66)	82.24 (0.98)	78.21 (0.92)	73.97 (1.22)
	$y_{\text{mt}} = 1, y_{\text{sp}} = 0$	81.74 (0.54)	79.66 (0.35)	76.46 (0.35)	70.93 (1.10)	63.42 (1.26)
	$y_{\text{mt}} = 1, y_{\text{sp}} = 1$	81.81 (0.31)	84.86 (0.46)	86.14 (0.86)	87.47 (0.42)	88.18 (0.96)
	Worst-group	81.38 (0.41)	79.66 (0.35)	76.46 (0.35)	70.93 (1.10)	63.42 (1.26)
	Average	84.59 (0.40)	84.42 (0.23)	83.80 (0.38)	82.28 (0.32)	79.88 (0.33)
ERM	$y_{\text{mt}} = 0, y_{\text{sp}} = 0$	87.42 (0.69)	88.99 (0.55)	91.06 (0.37)	94.30 (0.43)	97.06 (0.29)
	$y_{\text{mt}} = 0, y_{\text{sp}} = 1$	87.20 (0.49)	83.73 (0.60)	80.48 (1.11)	70.24 (1.91)	51.84 (3.09)
	$y_{\text{mt}} = 1, y_{\text{sp}} = 0$	81.87 (0.48)	79.65 (0.34)	75.84 (0.27)	65.92 (1.84)	52.05 (1.37)
	$y_{\text{mt}} = 1, y_{\text{sp}} = 1$	81.92 (0.31)	85.39 (0.55)	87.57 (0.59)	91.60 (0.66)	96.13 (0.70)
	Worst-group	81.50 (0.35)	79.65 (0.34)	75.84 (0.27)	65.26 (1.72)	49.70 (2.22)
	Average	84.60 (0.39)	84.44 (0.24)	83.74 (0.31)	80.52 (0.62)	74.27 (0.73)
INLP	$y_{\text{mt}} = 0, y_{\text{sp}} = 0$	87.44 (0.69)	88.96 (0.57)	90.50 (0.41)	95.09 (4.41)	56.45 (1.77)
	$y_{\text{mt}} = 0, y_{\text{sp}} = 1$	87.20 (0.49)	83.84 (0.63)	81.95 (0.77)	65.95 (4.04)	58.26 (4.10)
	$y_{\text{mt}} = 1, y_{\text{sp}} = 0$	81.86 (0.49)	79.73 (0.33)	76.51 (0.34)	62.10 (4.29)	50.64 (3.92)
	$y_{\text{mt}} = 1, y_{\text{sp}} = 1$	81.94 (0.32)	85.30 (0.52)	86.43 (0.67)	63.12 (7.22)	54.54 (3.12)
	Worst-group	81.47 (0.36)	79.73 (0.33)	76.51 (0.34)	57.62 (4.97)	48.13 (3.12)
	Average	84.61 (0.39)	84.46 (0.22)	83.85 (0.36)	66.56 (4.51)	54.97 (2.06)
RLACE	$y_{\text{mt}} = 0, y_{\text{sp}} = 0$	87.16 (0.72)	88.90 (0.47)	81.89 (0.82)	76.61 (1.60)	69.33 (1.95)
	$y_{\text{mt}} = 0, y_{\text{sp}} = 1$	87.24 (0.55)	84.02 (0.72)	91.09 (0.39)	92.02 (0.69)	93.70 (0.38)
	$y_{\text{mt}} = 1, y_{\text{sp}} = 0$	81.64 (0.51)	79.81 (0.31)	84.59 (1.12)	86.27 (0.87)	88.90 (1.04)
	$y_{\text{mt}} = 1, y_{\text{sp}} = 1$	82.16 (0.32)	85.01 (0.43)	72.16 (1.18)	66.69 (1.51)	61.15 (1.20)
	Worst-group	81.52 (0.44)	79.81 (0.31)	72.16 (1.18)	66.69 (1.51)	61.15 (1.20)
	Average	84.55 (0.43)	84.43 (0.25)	82.43 (0.35)	80.40 (0.64)	78.27 (0.41)

Table 3: **Results for the MultiNLI dataset:** Table shows the average, worst-group, and per-group accuracy on a test set where $p_{\text{OOD}}(y_{\text{mt}} = y | y_{\text{sp}} = y) = 0.5$, with $y \in \{0, 1\}$, as a function of $p_{\text{train}}(y_{\text{mt}} = y | y_{\text{sp}} = y)$. Each accuracy is obtained by averaging over 5 runs. Standard error is reported between brackets.

Method	Accuracy	ρ				
		0.0	0.1	0.2	0.3	0.4
JSE	$y_{mt} = 0, y_{sp} = 0$	83.71 (0.17)	83.62 (0.18)	83.46 (0.18)	83.36 (0.18)	83.40 (0.16)
	$y_{mt} = 0, y_{sp} = 1$	83.67 (0.16)	83.56 (0.17)	83.36 (0.19)	83.31 (0.18)	83.24 (0.19)
	$y_{mt} = 1, y_{sp} = 0$	83.73 (0.19)	83.71 (0.20)	83.79 (0.19)	83.71 (0.18)	83.63 (0.20)
	$y_{mt} = 1, y_{sp} = 1$	83.77 (0.15)	83.83 (0.16)	83.81 (0.16)	83.84 (0.17)	83.82 (0.17)
	Worst-group	81.95 (0.12)	81.86 (0.13)	81.81 (0.13)	81.82 (0.13)	81.68 (0.12)
	Average	83.73 (0.09)	83.69 (0.09)	83.61 (0.09)	83.56 (0.09)	83.53 (0.09)
ERM	$y_{mt} = 0, y_{sp} = 0$	83.55 (0.16)	83.46 (0.18)	83.42 (0.19)	83.52 (0.21)	83.85 (0.23)
	$y_{mt} = 0, y_{sp} = 1$	83.82 (0.17)	83.73 (0.17)	83.38 (0.19)	83.17 (0.22)	82.44 (0.29)
	$y_{mt} = 1, y_{sp} = 0$	83.89 (0.19)	83.83 (0.20)	83.72 (0.20)	83.50 (0.21)	82.82 (0.35)
	$y_{mt} = 1, y_{sp} = 1$	83.61 (0.16)	83.72 (0.16)	83.83 (0.16)	83.92 (0.20)	84.22 (0.21)
	Worst-group	81.90 (0.13)	81.80 (0.13)	81.63 (0.13)	81.41 (0.15)	80.72 (0.25)
	Average	83.74 (0.08)	83.70 (0.08)	83.60 (0.09)	83.54 (0.09)	83.35 (0.10)
INLP	$y_{mt} = 0, y_{sp} = 0$	83.76 (0.18)	83.07 (0.29)	78.93 (0.80)	72.41 (1.16)	64.74 (1.17)
	$y_{mt} = 0, y_{sp} = 1$	83.64 (0.17)	83.44 (0.24)	80.08 (0.74)	74.74 (1.10)	67.58 (1.24)
	$y_{mt} = 1, y_{sp} = 0$	83.60 (0.22)	83.66 (0.25)	80.52 (0.73)	75.42 (1.08)	68.16 (1.21)
	$y_{mt} = 1, y_{sp} = 1$	83.79 (0.16)	83.43 (0.23)	79.52 (0.82)	72.99 (1.14)	65.16 (1.16)
	Worst-group	81.72 (0.14)	81.26 (0.24)	77.32 (0.81)	70.58 (1.19)	61.41 (1.24)
	Average	83.70 (0.09)	83.41 (0.18)	79.77 (0.75)	73.90 (1.09)	66.45 (1.11)
RLACE	$y_{mt} = 0, y_{sp} = 0$	83.69 (0.21)	81.44 (0.23)	78.52 (0.26)	75.37 (0.26)	72.31 (0.27)
	$y_{mt} = 0, y_{sp} = 1$	83.49 (0.20)	85.42 (0.18)	86.90 (0.17)	88.25 (0.14)	89.08 (0.13)
	$y_{mt} = 1, y_{sp} = 0$	83.57 (0.25)	85.43 (0.23)	87.13 (0.18)	88.47 (0.16)	89.42 (0.14)
	$y_{mt} = 1, y_{sp} = 1$	83.60 (0.21)	81.67 (0.25)	79.27 (0.26)	75.98 (0.28)	72.99 (0.28)
	Worst-group	81.20 (0.16)	80.30 (0.21)	77.72 (0.24)	74.53 (0.25)	71.38 (0.25)
	Average	83.59 (0.09)	83.49 (0.09)	82.96 (0.10)	82.02 (0.11)	80.95 (0.11)

Table 4: **Results for the Toy dataset for $\rho \in \{0.0, 0.1, 0.2, 0.3, 0.4\}$.** Table shows the average, worst-group, and per-group accuracy on a test set without spurious correlation, as a function of the spurious correlation in the training data. Each accuracy is obtained by averaging over 100 runs. Standard error is reported between brackets.

Method	Accuracy	ρ				
		0.5	0.6	0.7	0.8	0.9
JSE	$y_{mt} = 0, y_{sp} = 0$	83.27 (0.16)	83.31 (0.17)	83.25 (0.18)	83.30 (0.18)	83.49 (0.26)
	$y_{mt} = 0, y_{sp} = 1$	83.20 (0.18)	83.06 (0.18)	82.99 (0.20)	83.06 (0.21)	81.87 (0.45)
	$y_{mt} = 1, y_{sp} = 0$	83.57 (0.20)	83.54 (0.21)	83.48 (0.22)	83.31 (0.20)	82.35 (0.47)
	$y_{mt} = 1, y_{sp} = 1$	83.67 (0.18)	83.71 (0.18)	83.76 (0.18)	83.65 (0.19)	84.05 (0.25)
	Worst-group	81.54 (0.12)	81.55 (0.13)	81.42 (0.14)	81.44 (0.14)	80.27 (0.42)
	Average	83.43 (0.09)	83.41 (0.10)	83.38 (0.09)	83.33 (0.10)	82.94 (0.18)
ERM	$y_{mt} = 0, y_{sp} = 0$	83.61 (0.22)	83.76 (0.27)	84.60 (0.31)	86.00 (0.31)	88.72 (0.28)
	$y_{mt} = 0, y_{sp} = 1$	82.76 (0.28)	82.10 (0.40)	80.39 (0.53)	77.80 (0.77)	69.97 (0.88)
	$y_{mt} = 1, y_{sp} = 0$	83.03 (0.30)	82.50 (0.42)	80.62 (0.60)	77.78 (0.79)	70.11 (0.94)
	$y_{mt} = 1, y_{sp} = 1$	83.93 (0.22)	84.16 (0.24)	84.97 (0.28)	85.99 (0.32)	88.86 (0.26)
	Worst-group	80.76 (0.22)	80.06 (0.36)	78.51 (0.53)	76.01 (0.77)	68.41 (0.91)
	Average	83.35 (0.09)	83.15 (0.12)	82.67 (0.17)	81.90 (0.26)	79.43 (0.35)
INLP	$y_{mt} = 0, y_{sp} = 0$	59.94 (1.03)	58.54 (0.90)	55.66 (0.81)	54.71 (0.68)	53.06 (0.69)
	$y_{mt} = 0, y_{sp} = 1$	62.83 (1.19)	61.77 (1.26)	58.31 (1.29)	56.64 (1.27)	56.01 (1.53)
	$y_{mt} = 1, y_{sp} = 0$	62.82 (1.19)	60.43 (1.31)	58.98 (1.26)	57.09 (1.26)	58.23 (1.48)
	$y_{mt} = 1, y_{sp} = 1$	60.52 (1.01)	57.87 (0.95)	56.60 (0.82)	55.09 (0.65)	55.14 (0.70)
	Worst-group	55.51 (1.06)	53.06 (0.95)	50.06 (0.77)	48.59 (0.55)	47.06 (0.56)
	Average	61.58 (0.94)	59.71 (0.89)	57.44 (0.76)	55.93 (0.68)	55.67 (0.74)
RLACE	$y_{mt} = 0, y_{sp} = 0$	68.59 (0.27)	64.77 (0.27)	60.84 (0.29)	57.30 (0.28)	53.89 (0.30)
	$y_{mt} = 0, y_{sp} = 1$	89.97 (0.14)	90.60 (0.13)	91.02 (0.12)	91.21 (0.13)	90.71 (0.30)
	$y_{mt} = 1, y_{sp} = 0$	90.22 (0.13)	90.87 (0.13)	91.30 (0.13)	91.65 (0.14)	90.89 (0.39)
	$y_{mt} = 1, y_{sp} = 1$	69.32 (0.33)	65.42 (0.31)	61.70 (0.31)	57.85 (0.32)	54.39 (0.35)
	Worst-group	67.65 (0.27)	63.87 (0.27)	59.74 (0.27)	55.89 (0.25)	52.31 (0.27)
	Average	79.53 (0.13)	77.92 (0.13)	76.22 (0.13)	74.50 (0.13)	72.48 (0.20)

Table 5: **Results for the Toy dataset for $\rho \in \{0.5, 0.6, 0.7, 0.8, 0.9\}$.** Table shows the average, worst-group, and per-group accuracy on a test set without spurious correlation, as a function of the spurious correlation in the training data. Each accuracy is obtained by averaging over 100 runs. Standard error is reported between brackets.

B ADDITIONAL RESULTS FOR TOY DATASET

B.1 REMOVING THE ORTHOGONALITY ASSUMPTION

In this section, we provide an analysis on how JSE performs when the \mathcal{Z}_{sp} and \mathcal{Z}_{mt} are not orthogonal subspaces. We create an example of the Toy dataset where the orthogonality assumption does not hold, by changing the angle of \mathbf{w}_{sp} and \mathbf{w}_{mt} to 75° . Let $a = \cos(\frac{15\pi}{180})$, $b = \sin(\frac{15\pi}{180})$, and $\mathbf{w}_{\text{sp}} = (\gamma, 0, 0, \dots, 0)^T$ and $\mathbf{w}_{\text{mt}} = (\frac{\gamma}{1+\frac{a}{b}}, \frac{\gamma}{1+\frac{b}{a}}, 0, \dots, 0)^T$. The main-task labels are now determined by a linear combination of the spurious and main-task directions. In Figure 8, we illustrate the subspaces found by JSE for this scenario. JSE finds a spurious and main-task vector that are slightly different from the basis vectors, yet orthogonal. This illustrates that when the \mathcal{Z}_{sp} and \mathcal{Z}_{mt} are not orthogonal subspaces, JSE finds two orthogonal subspaces that best fit given the data.

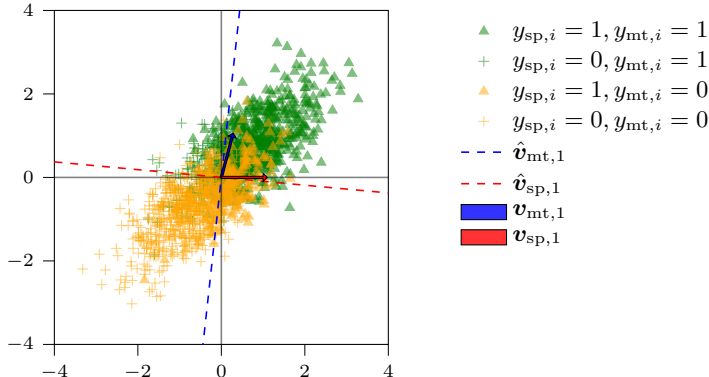


Figure 8: **Illustration of vectors found by JSE with non-orthogonal spurious and main-task subspaces:** The blue and red arrow indicate the basis of the spurious and main-task subspaces, which have an angle of 75° . Data is based on a single simulation from the $d(= 20)$ -dimensional Toy dataset of Section 4.1 with $\rho = 0.8$ and sample size $n = 2,000$.

Figure 9 shows the performance for the toy dataset when the subspaces are not orthogonal. Compared to the case where the subspaces are orthogonal, the performance of JSE is slightly worse. It removes a small part of the main-task direction, and leaves a small part of the spurious direction. However, it still outperforms other concept-removal methods such as INLP and RLACE. These methods perform relatively worse, because they also remove part of the main-task direction - even when there is no correlation between the spurious and main-task direction. When the spurious direction is removed, the part of the main-task direction that is non-orthogonal to it is also removed.

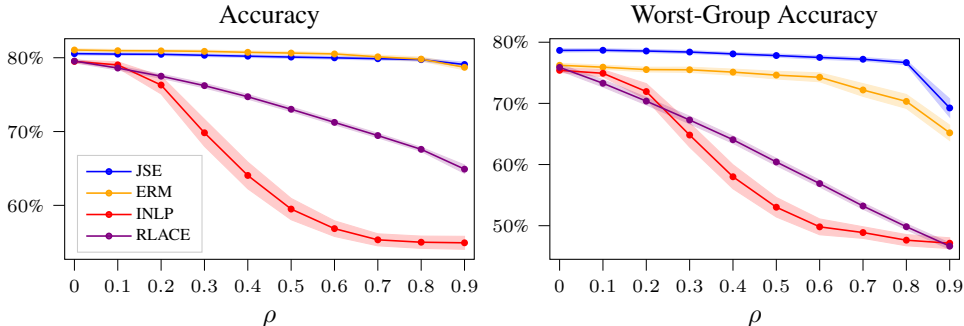


Figure 9: **OOD generalization for Toy dataset, when the angle between the spurious and main-task vector is 75° :** We plot the (worst-group) accuracy on a test set without spurious correlation, as a function of the spurious correlation in the training data. Each accuracy is obtained by averaging over 100 runs. The shaded area reflects the 95% confidence interval.

B.2 FINITE-SAMPLE ESTIMATION NOISE FOR JSE AND INLP

In this section, we briefly illustrate how the performance of JSE and INLP is affected by the interaction of (i) the size of the training set, and (ii) the correlation between the spurious and main-task features. Figure 10 shows the result of applying JSE and INLP to the Toy dataset for different sizes of the dataset. For JSE, we observe that with a limited sample size and a high spurious correlation, it is harder to separate the spurious and main-task features. We attribute this to finite-sample noise: our method finds two orthogonal vectors that fit well in the training data, but they are less likely to align with the data-generating process. Interestingly, INLP becomes worse as the sample size increases. With a greater sample size, it is more likely that INLP assigns the main-task feature as belonging to the spurious subspace, since its predictive ability of the spurious concept label is more likely to be detected.

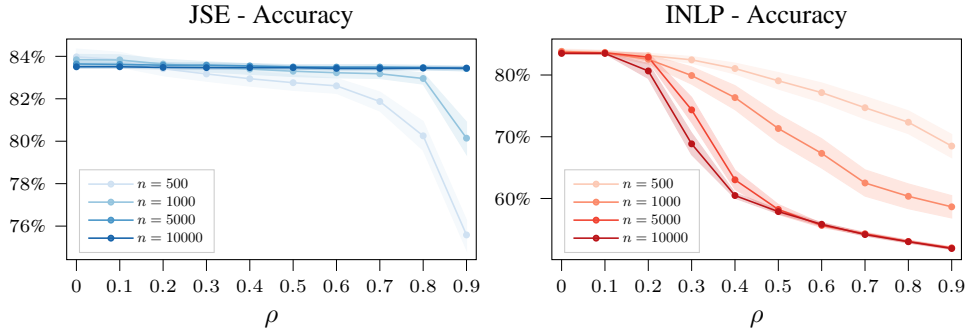


Figure 10: **Effect of training set size and spurious correlation strength for Toy dataset:** We plot the accuracy on a test set without spurious correlation, as a function of the spurious correlation in the training data. Each accuracy is obtained by averaging over 100 runs. The shaded area reflects the 95% confidence interval.

C THE JSE ALGORITHM

In this section, we first provide a more detailed version of the JSE algorithm, initially described in Section 3.2. We briefly investigate two modifications of the algorithm.

C.1 DETAILED DESCRIPTION OF THE JSE ALGORITHM

In Equation 2 we note that we optimize over the coefficients for two logistic regressions, while enforcing an orthogonality constraint. Here, we briefly explain how this constraint is enforced. We solve the following unconstrained problem using stochastic gradient descent (SGD):

$$\hat{\mathbf{w}}_{\text{sp}}, \hat{\mathbf{w}}_{\text{mt}}, \hat{b}_{\text{sp}}, \hat{b}_{\text{mt}} = \arg \min_{\mathbf{w}_{\text{sp}}, \mathbf{w}_{\text{mt}}, b_{\text{sp}}, b_{\text{mt}}} \sum_{i=1}^n \mathcal{L}_{\text{BCE}}(\hat{y}_{\text{sp},i}, y_{\text{sp},i}) + \mathcal{L}_{\text{BCE}}(\hat{y}_{\text{mt},i}, y_{\text{mt},i}),$$

where we define the predictions as follows:

$$\begin{aligned} \hat{y}_{\text{sp},i} &= \text{Logit}^{-1}(\mathbf{z}_i^T \mathbf{w}_{\text{sp}} + b_{\text{sp}}), \\ \hat{y}_{\text{mt},i} &= \text{Logit}^{-1}(\mathbf{z}_i^T (\mathbf{I} - \mathbf{P}_{\mathbf{w}_{\text{sp}}}) \mathbf{w}_{\text{mt}} + b_{\text{mt}}), \\ \mathbf{P}_{\mathbf{w}_{\text{sp}}} &= \mathbf{w}_{\text{sp}} (\mathbf{w}_{\text{sp}}^T \mathbf{w}_{\text{sp}})^{-1} \mathbf{w}_{\text{sp}}^T. \end{aligned}$$

By definition, $(\mathbf{I} - \mathbf{P}_{\mathbf{w}_{\text{sp}}}) \mathbf{w}_{\text{mt}}$ is orthogonal to \mathbf{w}_{sp} . Therefore, the predictions for each $y_{\text{mt},i}$ are based upon a set of coefficients that is orthogonal to \mathbf{w}_{sp} . By weighing both losses equally, there is no reason for this optimization problem to favor the loss for one set of labels over the other.

In Algorithm 2 we provide the exact same procedure as in Algorithm 1, but in greater detail.

Algorithm 2 JSE algorithm to estimate orthonormal bases for \mathcal{Z}_{sp} and \mathcal{Z}_{mt} . The calculation of the test statistics is discussed in Section D.3

Require: a sample $\{y_{\text{mt},i}, y_{\text{sp},i}, \mathbf{z}_i\}_{i=1}^n$ consisting of two binary labels and a vector $\mathbf{z}_i \in \mathbb{R}^d$.

Initialize a $(n \times d)$ -dimensional embedding matrix $\mathbf{Z} = (\mathbf{z}_1 \mathbf{z}_2 \cdots \mathbf{z}_n)^T$.

Initialize $\mathbf{Z}_{\text{sp}}^\perp \leftarrow \mathbf{Z}$.

Choose a significance level α for the test statistics, resulting in critical value $t_{1-\alpha}$

for $i = 1, \dots, d$ **do**

$\mathbf{Z}_{\text{remain}} \leftarrow \mathbf{Z}_{\text{sp}}^\perp$

for $j = 1, \dots, d$ **do**

 Estimate $\hat{\mathbf{w}}_{\text{sp}}$ and $\hat{\mathbf{w}}_{\text{mt}}$ with Equation 2, using embeddings $\mathbf{Z}_{\text{remain}}$.

 Define normalizations $\hat{\mathbf{v}}_{\text{sp},i} \leftarrow \hat{\mathbf{w}}_{\text{sp}} / \|\hat{\mathbf{w}}_{\text{sp}}\|$ and $\hat{\mathbf{v}}_{\text{mt},j} \leftarrow \hat{\mathbf{w}}_{\text{mt}} / \|\hat{\mathbf{w}}_{\text{mt}}\|$.

 Estimate $\hat{\gamma}_{\text{sp}}, \hat{b}_{\text{sp}} = \arg \min_{\gamma_{\text{sp}}, b_{\text{sp}}} \sum_{h=1}^n \mathcal{L}_{\text{BCE}}(\hat{y}_{\text{sp},h}^{(\hat{\mathbf{v}}_{\text{mt},j})}, y_{\text{sp},h})$,

 where $\hat{y}_{\text{sp},h}^{(\hat{\mathbf{v}}_{\text{mt},j})} = \text{Logit}^{-1}(\gamma_{\text{sp}} \mathbf{z}_{h,\text{remain}}^T \hat{\mathbf{v}}_{\text{mt},j} + b_{\text{sp}})$

 Calculate $t_{\text{mt},\text{rnd}}, t_{\text{mt},\text{sp}}^{(\hat{\mathbf{v}}_{\text{mt},j})}$ (see Section D.3)

if $(t_{\text{mt},\text{rnd}} < -t_{1-\alpha})$ and $(t_{\text{mt},\text{sp}}^{(\hat{\mathbf{v}}_{\text{mt},j})} > t_{1-\alpha})$ **then**

 Projection $\mathbf{Z}_{\text{remain}} \leftarrow \mathbf{Z}_{\text{sp}}^\perp (\mathbf{I} - \hat{\mathbf{V}}_{\text{mt}} \hat{\mathbf{V}}_{\text{mt}}^T)$, where $\hat{\mathbf{V}}_{\text{mt}} = (\hat{\mathbf{v}}_{\text{mt},1} \hat{\mathbf{v}}_{\text{mt},2} \cdots \hat{\mathbf{v}}_{\text{mt},j})$

else

break

end if

end for

 Estimate $\hat{\gamma}_{\text{mt}}, \hat{b}_{\text{mt}} = \sum_{h=1}^n \arg \min_{\gamma_{\text{mt}}, b_{\text{mt}}} \mathcal{L}_{\text{BCE}}(\hat{y}_{\text{mt},h}^{(\hat{\mathbf{v}}_{\text{sp},i})}, y_{\text{mt},h})$,

 where $\hat{y}_{\text{mt},h}^{(\hat{\mathbf{v}}_{\text{sp},i})} = \text{Logit}^{-1}(\gamma_{\text{mt}} \mathbf{z}_{h,\text{sp}}^T \hat{\mathbf{v}}_{\text{sp},i} + b_{\text{mt}})$

 Calculate $t_{\text{sp},\text{rnd}}, t_{\text{mt},\text{sp}}^{(\hat{\mathbf{v}}_{\text{sp},i})}$ (see Section D.3)

if $(t_{\text{sp},\text{rnd}} < -t_{1-\alpha})$ and $(t_{\text{mt},\text{sp}}^{(\hat{\mathbf{v}}_{\text{sp},i})} < -t_{1-\alpha})$ **then**

 Projection $\mathbf{Z}_{\text{sp}}^\perp \leftarrow \mathbf{Z} (\mathbf{I} - \hat{\mathbf{V}}_{\text{sp}} \hat{\mathbf{V}}_{\text{sp}}^T)$, where $\hat{\mathbf{V}}_{\text{sp}} = (\hat{\mathbf{v}}_{\text{sp},1} \hat{\mathbf{v}}_{\text{sp},2} \cdots \hat{\mathbf{v}}_{\text{sp},i})$.

else

break

end if

end for

return $\hat{\mathbf{v}}_{\text{sp},1}, \hat{\mathbf{v}}_{\text{sp},2}, \dots, \hat{\mathbf{v}}_{\text{sp},i}$

C.2 MODIFICATIONS OF THE JSE ALGORITHM

In this section, we briefly compare the formulation of the JSE algorithm to two alternatives.

- **Swapping the loops:** one might consider interchanging the inner loop and the outer loop of the JSE algorithm. Now, at each step, first the spurious vectors $\hat{\mathbf{v}}_{\text{sp},1}, \hat{\mathbf{v}}_{\text{sp},2}, \dots, \hat{\mathbf{v}}_{\text{sp},d_{\text{sp}}}$ are projected out before the main-task vector (at that step) is estimated.
- **Projecting onto main-task subspace:** instead of projecting \mathbf{z} onto the orthogonal complement of \mathcal{Z}_{sp} , one could be interested in projecting onto \mathcal{Z}_{mt} . In this case, rather than the transformation $(\mathbf{I} - \mathbf{V}_{\text{sp}} \mathbf{V}_{\text{sp}}^T) \mathbf{z}$, one uses the transformed embeddings $(\mathbf{V}_{\text{mt}} \mathbf{V}_{\text{mt}}^T) \mathbf{z}$.

In Table 6 we compare these two alternative formulations of the algorithm for the Waterbirds dataset. The performance for these two versions is similar to the JSE algorithm as outlined in Section 3.2,

although we observe a small drop in worst-group accuracy for the version with switched for-loops. We suggest that in practice, which version of the algorithm should be used could depend on (1) whether the user wants to remove a certain spurious concept, or isolate certain main-task features, and (2) the dimensionality of both subspaces. For example, if the dimension of the main-task subspace is much lower than that of the spurious concept subspace, it might be worthwhile to project onto z_{mt} to improve the bias-variance trade-off, rather than removing z_{sp} .

Method	Accuracy	$p_{\text{train}}(y_{\text{mt}} = y y_{\text{sp}} = y)$				
		0.5	0.6	0.7	0.8	0.9
JSE with projecting onto z_{mt}	$y_{\text{mt}} = 0, y_{\text{sp}} = 0$	93.40 (0.15)	91.55 (0.80)	91.44 (0.37)	91.60 (0.31)	89.24 (0.87)
	$y_{\text{mt}} = 0, y_{\text{sp}} = 1$	89.81 (0.20)	87.69 (0.98)	87.79 (0.46)	89.62 (0.40)	86.72 (1.00)
	$y_{\text{mt}} = 1, y_{\text{sp}} = 0$	90.58 (0.11)	91.60 (0.26)	91.89 (0.15)	91.64 (0.14)	92.00 (0.22)
	$y_{\text{mt}} = 1, y_{\text{sp}} = 1$	90.99 (0.16)	91.63 (0.25)	91.84 (0.16)	91.47 (0.13)	90.94 (0.33)
	Worst-group	89.63 (0.17)	87.67 (0.97)	87.79 (0.46)	89.53 (0.38)	86.50 (0.96)
	Average	91.42 (0.10)	90.06 (0.64)	90.11 (0.29)	90.82 (0.23)	88.75 (0.64)
JSE with Swapped Loops	$y_{\text{mt}} = 0, y_{\text{sp}} = 0$	92.77 (0.16)	90.88 (0.65)	90.26 (0.34)	91.58 (0.48)	93.13 (0.23)
	$y_{\text{mt}} = 0, y_{\text{sp}} = 1$	89.50 (0.23)	88.31 (0.68)	88.08 (0.56)	87.84 (0.38)	83.11 (0.95)
	$y_{\text{mt}} = 1, y_{\text{sp}} = 0$	90.76 (0.13)	91.63 (0.24)	92.02 (0.10)	91.12 (0.24)	90.13 (0.21)
	$y_{\text{mt}} = 1, y_{\text{sp}} = 1$	91.71 (0.14)	91.79 (0.21)	91.88 (0.24)	92.22 (0.26)	93.00 (0.33)
	Worst-group	89.42 (0.22)	88.26 (0.68)	88.01 (0.55)	87.47 (0.35)	83.10 (0.94)
	Average	91.16 (0.12)	90.06 (0.48)	89.79 (0.28)	90.15 (0.16)	88.89 (0.32)

Table 6: **Results for the Waterbirds dataset for different versions of the JSE algorithm:** Table shows the average, worst-group, and per-group accuracy on a test set where $p_{\text{OOD}}(y_{\text{mt}} = y | y_{\text{sp}} = y) = 0.5$, with $y \in \{0, 1\}$. Each accuracy is obtained by averaging over 20 runs. Standard error is reported between brackets.

D DETAILS ON THE TESTING PROCEDURE OF JSE

In this section, we provide a detailed explanation of the testing procedure used in the JSE algorithm for breaking the for-loops. Section D.1 will introduce notation, and a general set-up that is applicable for each test. In Section D.2 we provide the derivations that are needed for our subsequent test statistics. In Section D.3 we define the test statistics that are used throughout the JSE method. In Section D.4 we study the effect of our choice to equally weight across the four groups in the data when measuring the test statistics, and in Section D.5 we investigate how one can adjust the test in cases where one set of labels is much harder to predict than the other.

D.1 NOTATION AND SET-UP

Recall from Section 3.3 that we are interested in testing the difference between two binary cross-entropies (BCE). For example, we can define the difference in BCE between a logistic regression that is trained on our embeddings z to predict the spurious concept labels y_{sp} and one that just uses an intercept (referred to as ‘random’ classifier).

For a particular sample, one could simply estimate this difference by weighting the individual observations equally. However, for our tests, we noticed that there was a considerable improvement if the difference was weighted equally within the subgroups specified by the pair of labels $(y_{\text{mt}}, y_{\text{sp}})$. This is examined in Section D.4. Below, we formulate how one, in general, can test for such a weighted difference between BCE’s of two classifiers.

Based on the main task and spurious labels $y_{\text{mt}}, y_{\text{sp}}$, we define four groups: (1) $y_{\text{mt}} = 0, y_{\text{sp}} = 0$, (2) $y_{\text{mt}} = 0, y_{\text{sp}} = 1$, (3) $y_{\text{mt}} = 1, y_{\text{sp}} = 0$, and (4) $y_{\text{mt}} = 1, y_{\text{sp}} = 1$. The spurious and main-task labels are used to define a new random variable $G \in \{1, 2, 3, 4\}$, indicating group membership. The probability of a group g is noted as π_g .

We consider the difference between the binary cross-entropy (BCE) as a random variable d . We assume that this difference is a mixture of four random variables: d_1, d_2, d_3, d_4 . The random variable d_g corresponds to the difference in BCE for group g . We assume that the expectation and variance of each of these four random variables is different, e.g. $\mathbb{E}[d_g] \neq \mathbb{E}[d_h], \text{Var}[d_g] \neq \text{Var}[d_h]$, for $g \neq h$. However, we do assume that they are independent: $\text{Cov}(d_g, d_h) = 0$. I denote the $\mathbb{E}[d_g] = \mu_g$ and $\text{Var}[d_g] = \sigma_g^2$.

We are interested in the weighted average of d_1, d_2, d_3, d_4 , where each group receives an equal weight. Concretely, we can define a new random variable

$$d_w = \frac{1}{4} \sum_{g=1}^4 d_g.$$

The subscript of w will be used to refer to the equally weighted sum of difference d . We are interested in the following hypotheses

$$H_0 : \mathbb{E}[d_w] = 0, \quad H_1 : \mathbb{E}[d_w] < 0.$$

We draw a sample of n independent and identical (IID) observations from d and G .

Because we observe G , we know for each observation which random variable we are observing - e.g. if $G = 1$, we observe d_1 . This means that after drawing the n observations, we observe the n_g observations for group g . The observations of d from group g are denoted as $d_{g,i}$ for $i = 1, 2, \dots, n_g$. However, we do not know the value of each π_g . We do assume each π_g is strictly positive.

D.2 DERIVATION OF TEST STATISTIC

The expectation of d_w is

$$\mu_w = \mathbb{E}[d_w] = \frac{1}{4} \mathbb{E} \left[\sum_{g=1}^4 d_g \right] = \frac{1}{4} \sum_{g=1}^4 \mu_g.$$

Let \bar{d}_w denote an estimator of d_w

$$\bar{d}_w = \frac{1}{4} \sum_{g=1}^4 \bar{d}_g, \quad \text{with } \bar{d}_g = \frac{1}{n_g} \sum_{i=1}^{n_g} d_{i,g},$$

where n_g is a random variable. We can show this estimator is unbiased via the law of total expectation.

$$\begin{aligned} \mathbb{E}[\bar{d}_g] &= \mathbb{E} \left[\frac{1}{n_g} \sum_{i=1}^{n_g} d_{i,g} \right] \\ &= \mathbb{E} \left[\mathbb{E} \left[\frac{1}{n_g} \sum_{i=1}^{n_g} d_{i,g} \mid n_g \right] \right] \\ &= \mathbb{E} \left[\frac{1}{n_g} \sum_{i=1}^{n_g} \mathbb{E}[d_{i,g} \mid n_g] \right] \\ &= \mathbb{E} \left[\frac{1}{n_g} n_g \mu_g \right] && \text{(Since they are IID)} \\ &= \mu_g, \\ \mathbb{E}[\bar{d}_w] &= \frac{1}{4} \sum_{g=1}^4 \mu_g. \end{aligned}$$

We now turn to the variance of \bar{d}_w

$$\begin{aligned} \text{Var}(\bar{d}_w) &= \text{Var} \left(\frac{1}{4} \sum_{g=1}^4 \bar{d}_g \right) \\ &= \frac{1}{16} \text{Var} \left(\sum_{g=1}^4 \bar{d}_g \right) \\ &= \frac{1}{16} \sum_{g=1}^4 \sum_{h=1}^4 \text{Cov}(\bar{d}_g, \bar{d}_h). \end{aligned}$$

First, it is shown first show that $\text{Cov}(\bar{d}_g, \bar{d}_h) = 0$ for $g \neq h$ via the law of total covariance:

$$\text{Cov}(\bar{d}_g, \bar{d}_h) = \mathbb{E}[\text{Cov}(\bar{d}_g, \bar{d}_h | n_g, n_h)] + \text{Cov}(\mathbb{E}[\bar{d}_g | n_g, n_h], \mathbb{E}[\bar{d}_h | n_g, n_h])$$

Since the sample means in expectation are the constants μ_g, μ_h , their covariance is 0:

$$\text{Cov}(\mathbb{E}[\bar{d}_g | n_g, n_h], \mathbb{E}[\bar{d}_h | n_g, n_h]) = \text{Cov}(\mu_g, \mu_h) = 0.$$

Next, we define

$$\begin{aligned} \mathbb{E}[\text{Cov}(\bar{d}_g, \bar{d}_h | n_g, n_h)] &= \mathbb{E} \left[\frac{1}{n_g} \frac{1}{n_h} \text{Cov} \left(\sum_{i=1}^{n_g} d_{i,g}, \sum_{i=1}^{n_h} d_{i,h} | n_g, n_h \right) \right] \\ &= \mathbb{E} \left[\frac{1}{n_g} \frac{1}{n_h} 0 \right] = 0, \end{aligned}$$

This last step can be made because we assume $d_{g,i}$ is independent of $d_{h,j}$ for $g \neq h, i = 1, \dots, n_g$ and $j = 1, \dots, n_h$. The variance of \bar{d}_w becomes

$$\text{Var}(\bar{d}_w) = \frac{1}{16} \sum_{g=1}^4 \text{Var}(\bar{d}_g).$$

We can define $\text{Var}(\bar{d}_g)$ via the law of total variance

$$\begin{aligned} \text{Var}(\bar{d}_g) &= \text{Var} \left(\frac{1}{n_g} \sum_{i=1}^{n_g} d_{i,g} \right) \\ &= \mathbb{E} \left[\text{Var} \left(\frac{1}{n_g} \sum_{i=1}^{n_g} d_{i,g} | n_g \right) \right] + \text{Var} \left(\mathbb{E} \left[\frac{1}{n_g} \sum_{i=1}^{n_g} d_{i,g} | n_g \right] \right) \\ &= \mathbb{E} \left[\text{Var} \left(\frac{1}{n_g} \sum_{i=1}^{n_g} d_{i,g} | n_g \right) \right] + \text{Var}(\mu_g) \\ &= \mathbb{E} \left[\text{Var} \left(\frac{1}{n_g} \sum_{i=1}^{n_g} d_{i,g} | n_g \right) \right] \quad (\text{Since variance of constant is 0}) \\ &= \mathbb{E} \left[\frac{1}{n_g^2} \sum_{i=1}^{n_g} \text{Var}(d_{i,g}) \right] \\ &= \mathbb{E} \left[\frac{1}{n_g^2} n_g \sigma_g^2 \right] \quad (\text{Since they are IID}) \\ &= \mathbb{E} \left[\frac{1}{n_g} \right] \sigma_g^2. \end{aligned}$$

For $n \rightarrow \infty$, n_g approximately follows a binomial distribution with $\mathbb{E}[n_g] = n\pi_g$ and variance $n\pi_g(1 - \pi_g)$. We define a second order Taylor expansion to approximate $\frac{1}{n_g}$ around $\mathbb{E}[n_g] = n\pi_g$

$$\mathbb{E} \left[\frac{1}{n_g} \right] \approx \frac{1}{n\pi_g} + \frac{(1 - \pi_g)}{n^2 \pi_g^2}.$$

This means:

$$\begin{aligned} \text{Var}(\bar{d}_g) &\approx \left(\frac{1}{n\pi_g} + \frac{(1 - \pi_g)}{n^2 \pi_g^2} \right) \sigma_g^2 \\ &= \frac{1}{n\pi_g} \sigma_g^2 + \mathcal{O}(n^{-2}). \end{aligned}$$

Using this, we approximate the variance of the weighted sum d_w via

$$\text{Var}(\bar{d}_w) \approx \frac{1}{16} \sum_{g=1}^4 \frac{1}{n\pi_g} \sigma_g^2.$$

Using the expectation and variance of \bar{d}_w , we now proceed to its asymptotic distribution. Assuming that (i) the sample means \bar{d}_g are based on IID random variables and (ii) σ_g^2 is bounded, we can use the central limit theorem (CLT) for each of the four sample means

$$\sqrt{n}(\bar{d}_g - \mu_g) \xrightarrow{d} \mathcal{N}(0, \frac{\sigma_g^2}{\pi_g}).$$

This holds because $\lim_{n \rightarrow \infty} n_g/n = \pi_g > 0$ for all g ; see for instance Rényi (1957). Given that the CLT holds for each sample mean, joint convergence follows by independence of the sample means. Hence, the distribution of the linear combination directly follows

$$\sqrt{n}(\bar{d}_w - \mathbb{E}[d_w]) = \frac{1}{4} \sum_{g=1}^4 \sqrt{n}(\bar{d}_g - \mu_g) \xrightarrow{d} \mathcal{N}\left(0, \frac{1}{16} \sum_{g=1}^4 \frac{\sigma_g^2}{\pi_g}\right).$$

Hence, the variance of \bar{d}_w

$$\text{Var}(\bar{d}_w) \approx \frac{1}{16} \sum_{g=1}^4 \frac{\sigma_g^2}{n\pi_g}$$

can be consistently estimated via

$$\widehat{\text{Var}}(\bar{d}_w) = \frac{1}{16} \sum_{g=1}^4 \frac{s_g^2}{n\hat{\pi}_g} = \frac{1}{16} \sum_{g=1}^4 \frac{s_g^2}{n_g},$$

with $\hat{\pi}_g = n_g/n$, and $s_g^2 = \frac{1}{n_g-1} \sum_{i=1}^{n_g} (d_{g,i} - \bar{d}_g)^2$. Using this, we can define a test statistic t_w , which for $n \rightarrow \infty$

$$t_w = \frac{\bar{d}_w - \mathbb{E}[d_w]}{\widehat{\text{Var}}(\bar{d}_w)} \xrightarrow{d} \mathcal{N}(0, 1).$$

D.3 TEST STATISTICS FOR JSE

In the previous section, we defined a test statistic for the equally weighted average of d . Here, we will use this derivation for the test statistics in the inner and outer loop of JSE.

We start with the first criterion, namely that the vector \mathbf{v}_{sp} (\mathbf{v}_{mt}) is informative about the spurious label (main-task label). This criterion is operationalised as follows: the \mathbf{v}_{sp} should contain more information about y_{sp} than a majority-rule ‘random classifier’. The coefficients for a logistic regression can be written as a combination of a unit vector and a scalar: $\mathbf{w} = \mathbf{v}\gamma$. Consider a logistic regression model $\hat{y}_{\text{sp}}^{(\mathbf{v}_{\text{sp}})} = \text{Logit}^{-1}(\gamma_{\text{sp}} \mathbf{z}^T \mathbf{v}_{\text{sp}} + b_{\text{sp}})$. This is a predictor for the label y_{sp} based on the embeddings projected onto \mathbf{v}_{sp} . Let $\hat{y}_{\text{sp}}^{(\text{rnd})}$ denote a random classifier. We can define the difference between these two classifiers as

$$d_{\text{sp,rnd}}^{(\mathbf{v}_{\text{sp}})} = \mathcal{L}_{\text{BCE}}(\hat{y}_{\text{sp}}^{(\mathbf{v}_{\text{sp}})}, y_{\text{sp}}) - \mathcal{L}_{\text{BCE}}(\hat{y}_{\text{sp}}^{(\text{rnd})}, y_{\text{sp}}).$$

The first criterion translates into the following hypothesis test

$$H_0 : \mathbb{E}[d_{w,\text{sp,rnd}}^{(\mathbf{v}_{\text{sp}})}] = 0 \quad \text{versus} \quad H_1 : \mathbb{E}[d_{w,\text{sp,rnd}}^{(\mathbf{v}_{\text{sp}})}] < 0,$$

which means that under the null hypothesis, there is no difference in the BCE of these two classifiers. Under the alternative hypothesis, the BCE of a random classifier is higher.

We use the following test statistic, where under the null hypothesis

$$t_{\text{sp,rnd}} = \frac{\bar{d}_{w,\text{sp,rnd}}^{(\mathbf{v}_{\text{sp}})}}{\text{Var}(\bar{d}_{w,\text{sp,rnd}}^{(\mathbf{v}_{\text{sp}})})} \xrightarrow{d} \mathcal{N}(0, 1).$$

The previous test can also be defined for a main-task vector \mathbf{v}_{mt} and main-task labels y_{mt} . Consider a logistic regression model $\hat{y}_{\text{mt}}^{(\mathbf{v}_{\text{mt}})} = \text{Logit}^{-1}(\gamma_{\text{mt}} \mathbf{z}^T \mathbf{v}_{\text{mt}} + b_{\text{mt}})$. The difference between the BCE of this classifier and a random classifier $\hat{y}_{\text{mt}}^{(\text{rnd})}$ is:

$$d_{\text{mt,rnd}}^{(\mathbf{v}_{\text{mt}})} = \mathcal{L}_{\text{BCE}}(\hat{y}_{\text{mt}}^{(\mathbf{v}_{\text{mt}})}, y_{\text{mt}}) - \mathcal{L}_{\text{BCE}}(\hat{y}_{\text{mt}}^{(\text{rnd})}, y_{\text{mt}}),$$

which we can use for the following hypotheses

$$H_0 : \mathbb{E}[d_{w,mt,rand}^{(\mathbf{v}_{mt})}] = 0 \quad \text{versus} \quad H_1 : \mathbb{E}[d_{w,mt,rand}^{(\mathbf{v}_{mt})}] < 0.$$

For these hypotheses, we define a test statistic similar to the previous one, only now for the main-task vector and labels

$$t_{mt,rand} = \frac{\bar{d}_{w,mt,rand}^{(\mathbf{v}_{mt})}}{\text{Var}(\bar{d}_{w,mt,rand}^{(\mathbf{v}_{mt})})} \xrightarrow{d} \mathcal{N}(0, 1).$$

We now turn to the second criterion, which is that the \mathbf{v}_{sp} is more predictive of the spurious concept than the main-task concept (and vice-versa for \mathbf{v}_{mt}). This criterion is operationalised as follows: The BCE of a spurious vector \mathbf{v}_{sp} should be lower for the spurious concept than the main-task, and the vice-versa. We compare the BCE's of $\hat{y}_{sp}^{(\mathbf{v}_{sp})}$ and $\hat{y}_{mt}^{(\mathbf{v}_{sp})} = \text{Logit}^{-1}(\gamma'_{mt} \mathbf{z}^T \mathbf{v}_{sp} + b'_{mt})$, where the latter is a predictor for the main-task label, based on the embeddings projected onto \mathbf{v}_{sp} . The model parameters γ_{mt} and b_{mt} are to be trained by minimizing the BCE. We define the difference

$$d_{sp,mt}^{(\mathbf{v}_{sp})} = \mathcal{L}_{\text{BCE}}(\hat{y}_{sp}^{(\mathbf{v}_{sp})}, y_{sp}) - \mathcal{L}_{\text{BCE}}(\hat{y}_{mt}^{(\mathbf{v}_{sp})}, y_{mt}),$$

and use this difference to test the following hypotheses

$$H_0 : \mathbb{E}[d_{w,sp,mt}^{(\mathbf{v}_{sp})}] = \Delta \quad \text{versus} \quad H_1 : \mathbb{E}[d_{w,sp,mt}^{(\mathbf{v}_{sp})}] < \Delta,$$

where the parameter Δ can be used to adjust for the fact that one label is harder to predict than the other. We give an example of its usefulness in Appendix D.5, and a heuristic for setting the parameter value. Under the null hypothesis, the difference in the BCE for the spurious concept and main-task labels, for a logistic regression based on the embeddings projected onto \mathbf{v}_{sp} , is Δ . We can use the following test statistic, where under the null hypothesis

$$t_{sp,mt}^{(\mathbf{v}_{sp})} = \frac{\bar{d}_{w,sp,mt}^{(\mathbf{v}_{sp})} - \Delta}{\text{Var}(\bar{d}_{w,sp,mt}^{(\mathbf{v}_{sp})})} \xrightarrow{d} \mathcal{N}(0, 1).$$

We can then conduct the same test, but now for the main-task vector \mathbf{v}_{mt} instead of \mathbf{v}_{sp} . Define $\hat{y}_{sp}^{(\mathbf{v}_{mt})} = \text{Logit}^{-1}(\gamma'_{sp} \mathbf{z}^T \mathbf{v}_{mt} + b'_{sp})$. This test uses the following difference

$$d_{sp,mt}^{(\mathbf{v}_{mt})} = \mathcal{L}_{\text{BCE}}(\hat{y}_{sp}^{(\mathbf{v}_{mt})}, y_{sp}) - \mathcal{L}_{\text{BCE}}(\hat{y}_{mt}^{(\mathbf{v}_{mt})}, y_{mt}),$$

and the hypotheses become

$$H_0 : \mathbb{E}[d_{w,sp,mt}^{(\mathbf{v}_{mt})}] = \Delta \quad \text{versus} \quad H_1 : \mathbb{E}[d_{w,sp,mt}^{(\mathbf{v}_{mt})}] > \Delta.$$

Under H_1 we now test if the difference is greater than Δ compared to the previous test. We use the following test statistic:

$$t_{sp,mt}^{(\mathbf{v}_{mt})} = \frac{\bar{d}_{w,sp,mt}^{(\mathbf{v}_{mt})} - \Delta}{\text{Var}(\bar{d}_{w,sp,mt}^{(\mathbf{v}_{mt})})} \xrightarrow{d} \mathcal{N}(0, 1).$$

For each of the test statistics, given a large enough sample size, we can acquire our critical values from the standard normal distribution for a given significance level α .

In general, we used the validation set for the test statistics in order to mitigate the effect of overfitting. Unless otherwise mentioned, we set $\alpha = 0.05$ and $\Delta = 0$.

D.4 WEIGHTED AVERAGE VS. UNWEIGHTED AVERAGE FOR TEST STATISTICS OF JSE

As stated in the previous section, we use a weighted average for the test statistics of JSE, where the difference in BCE's is weighted equally across the four combinations of y_{sp} and y_{mt} . We argue that this is helpful in distinguishing whether or not a spurious concept vector \mathbf{v}_{sp} contains a spurious concept or not (vice versa for \mathbf{v}_{mt}).

For example, consider a sample where 90% of the water or landbirds coincide with a water or land background ($p_{\text{train}}(y_{\text{mt}} = y|y_{\text{sp}} = y) = 0.9$), and we are interested in determining if a vector v contains information about the spurious or main-task features. If v contains information about the background features, a logistic regression for the label y_{sp} based on the embeddings projected onto v will have a low BCE for spurious concept labels. However, this logistic regression will likely also have a low BCE for the main-task labels, due to the overlap between the labels. We can address this problem by weighting the BCE equally across the four combinations of y_{sp} and y_{mt} , where the groups with a small sample (and where y_{sp} and y_{mt} do not coincide) will have a greater influence on the overall average

We verify this argument empirically by comparing two versions of JSE: one with the equally weighted average for the test statistics (as presented in this paper), and one which uses a simple average. Figure 11 shows the results of applying these two versions of the JSE algorithm to the Waterbirds dataset. When the spurious correlation is high, the version with a simple average performs worse in terms of both overall and worst-group accuracy.

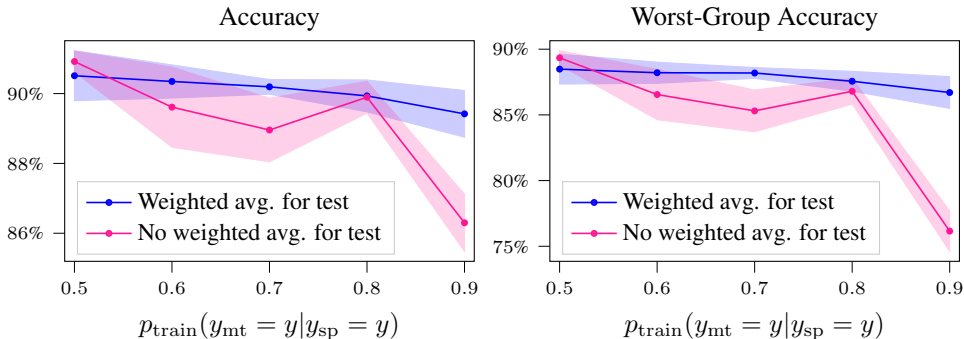


Figure 11: **Effect of using an equally weighted average for the tests of JSE for the Waterbirds dataset:** We plot the (worst-group) accuracy on an OOD test set where $p_{\text{OOD}}(y_{\text{mt}} = y|y_{\text{sp}} = y) = 0.5$, as a function of $p_{\text{train}}(y_{\text{mt}} = y|y_{\text{sp}} = y)$. Each accuracy is obtained by averaging over 20 runs. The shaded area reflects the 95% confidence interval.

D.5 ADJUSTING FOR DIFFERENT DIFFICULTY IN PREDICTING LABELS

A potential issue with comparing two BCE’s is that it might be fundamentally harder to predict one set of labels over the other. Consider the example of distinguishing cows vs. penguins as given in the introduction. If it is much easier to predict the background than the animal type, then we might wrongly attribute main-task vectors to \mathcal{Z}_{mt} . If the spurious concept is always easier to predict, then even if v represents the main-task features (e.g. the animal shape), the vector might be attributed to the spurious concept subspace, since it has a lower binary cross-entropy for the spurious concept label than the main task label.

To address this, we add the Δ term when testing for the second criterion mentioned in Section 3.3. By having a non-zero Δ , we can account for the fact that one binary cross-entropy is always likely to be lower (or higher) than the other.

This naturally leads to the question how one should determine Δ . We provide a simple heuristic. First, we optimize Equation 2 and obtain a first pair of spurious and main-task vectors, $\hat{v}_{\text{sp}}, \hat{v}_{\text{mt}}$. We compare the difference between these two orthogonal vectors through measuring the following:

$$d_{\text{sp,mt}}^* = \mathcal{L}_{\text{BCE}}(\hat{y}_{\text{sp}}^{\hat{v}_{\text{sp}}}, y_{\text{sp}}) - \mathcal{L}_{\text{BCE}}(\hat{y}_{\text{mt}}^{\hat{v}_{\text{mt}}}, y_{\text{mt}}).$$

We measure the weighted average of this term, defined $\bar{d}_{w,\text{sp,mt}}^*$, for the validation set. This gives an indication if one set of labels is harder to predict than the other, and its value can be used to set Δ .

In order to demonstrate the usefulness of Δ and the heuristic, consider the Toy dataset, outlined Section 4.1. In the original set-up, both sets of labels were equally hard to predict, since $\gamma_{\text{sp}} = \gamma_{\text{mt}} = 3$ for both. We change that for this section, and set $\gamma_{\text{sp}} = 6, \gamma_{\text{mt}} = 2$, making the spurious concept labels much more separable than the main-task labels.

In Figure 12 we show how JSE performs on a Toy dataset where the separability of the spurious and main-task labels differs. When we do not adjust Δ (e.g. keep it 0), we observe that both overall and worst-group accuracy drop once the correlation between the spurious and main-task features becomes high ($\rho = 0.9$). If we adjust Δ via our heuristic, this problem is avoided.

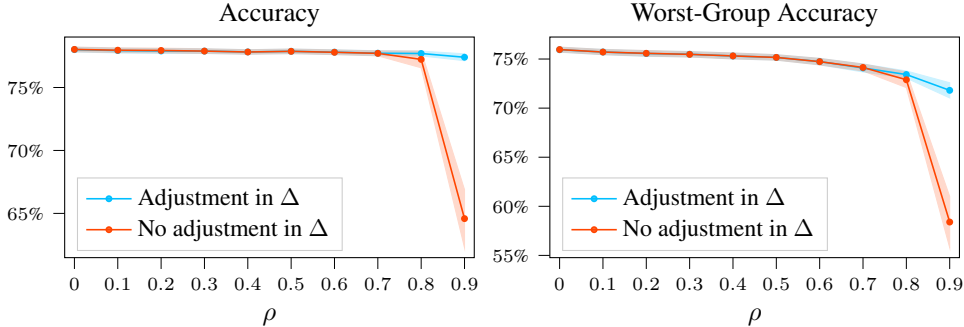


Figure 12: **Effect of adjusting Δ for JSE:** We plot the (worst-group) accuracy on a test set without spurious correlation, as a function of the spurious correlation in the training data. Each accuracy is obtained by averaging over 100 runs. The shaded area reflects the 95% confidence interval.

E COMPARISON TO GROUP-WEIGHTED ERM

In this section, we provide a comparison of JSE with group-weighted (GW) ERM. When focusing on the last layer of the neural network, an alternative to JSE is to sample in each batch such that in expectation, $p(y_{\text{mt}} = y | y_{\text{sp}} = y) = 0.5$, and $p(y_{\text{mt}} = y) = 0.5$ (Izmailov et al., 2022; Kirichenko et al., 2023; Idrissi et al., 2022). While this is a potentially useful method for dealing with spurious correlations, we argue that JSE addresses a different problem by focusing on the dependence between the spurious and main-task features, rather than the labels.

GW ERM addresses cases where in the OOD data, the conditional distribution $p_{\text{train}}(y_{\text{mt}} = y | y_{\text{sp}} = y) \neq p_{\text{OOD}}(y_{\text{mt}} = y | y_{\text{sp}} = y)$ e.g. the probability of a landbird appearing on water changes between the training and OOD data. However, group-weighted ERM can fail when the change between the training and OOD data is not in the conditional distribution $p(y_{\text{mt}} | y_{\text{sp}})$, but rather in the joint distribution $p(\mathbf{x}_{\text{mt}}, \mathbf{x}_{\text{sp}})$. If one has a sample where $p(y_{\text{mt}} | y_{\text{sp}}) = 0.5$, this does not mean that the main-task and spurious features become independent, i.e. $p(\mathbf{x}_{\text{mt}}, \mathbf{x}_{\text{sp}}) = p(\mathbf{x}_{\text{mt}})p(\mathbf{x}_{\text{sp}})$.

We provide a concrete example of this with the Toy dataset. In Figure 13, we show results for JSE and GW ERM for the Toy dataset, as outlined in Section 4.1. GW ERM performs worse than JSE for this dataset. We illustrate why this is the case in Figure 14. GW ERM does not find a decision boundary that is parallel to the spurious feature, since despite reweighting there is still a correlation between the main-task and spurious features.

When comparing JSE and group-weighted (GW) ERM for the Waterbirds dataset, we observe that the average accuracy of JSE is not significantly lower than that of group-weighted ERM, but JSE has a slightly lower worst-group accuracy. For CelebA, JSE is marginally worse in terms of both average and worst-group accuracy. For MultiNLI, we observe that the performance of both JSE and GW ERM decreases as the spurious correlation increases. We argue that the marginally better performance of GW ERM on these datasets is because in our experiments, we exactly simulate the situation that is suitable for GW ERM. Namely, we change the conditional distribution $p(y_{\text{mt}} = y | y_{\text{sp}} = y)$ between the training and test set, and we do not directly change the joint distribution $p(\mathbf{x}_{\text{mt}}, \mathbf{x}_{\text{sp}})$ of main-task and spurious features. This is because direct access to $p(\mathbf{x}_{\text{mt}}, \mathbf{x}_{\text{sp}})$ is not possible for these datasets. Recall that for the dataset where this is possible, namely the Toy dataset, JSE significantly outperforms GW ERM.

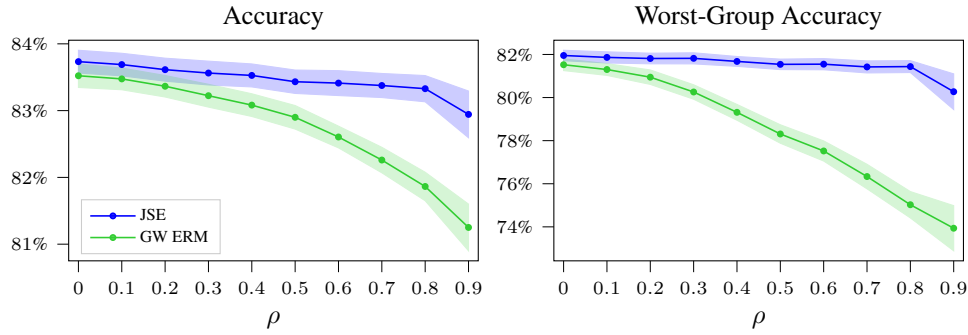


Figure 13: **Comparing JSE and group-weighted (GW) ERM for Toy dataset:** We plot the (worst-group) accuracy on a test set without spurious correlation, as a function of the spurious correlation in the training data. Each accuracy is obtained by averaging over 100 runs. The shaded area reflects the 95% confidence interval.

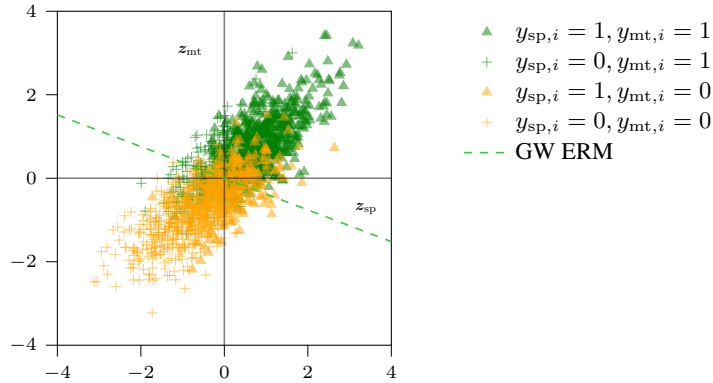


Figure 14: **Decision boundary for group-weighted (GW) ERM:** Data is from a single simulation from the $d(=20)$ -dimensional Toy dataset of Section 4.1 with $\rho = 0.8$ and sample size $n = 2,000$.

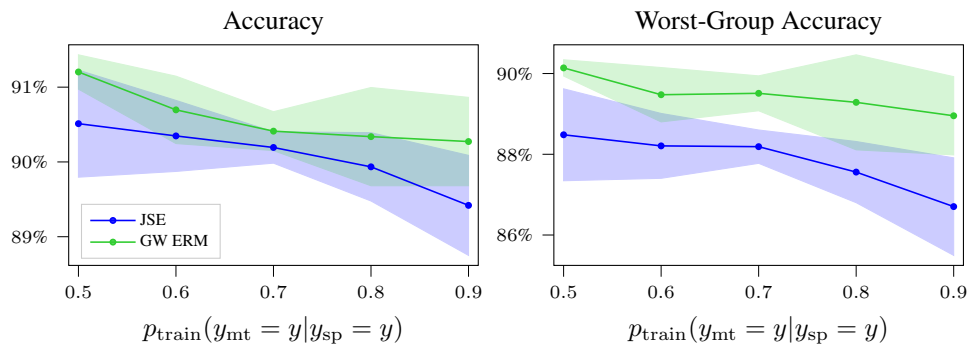


Figure 15: **Comparing JSE and group-weighted (GW) ERM for Waterbirds dataset:** We plot the (worst-group) accuracy on an OOD test set where $p_{\text{OOD}}(y_{mt} = y | y_{sp} = y) = 0.5$, as a function of $p_{\text{train}}(y_{mt} = y | y_{sp} = y)$. Each accuracy is obtained by averaging over 20 runs. The shaded area reflects the 95% confidence interval.

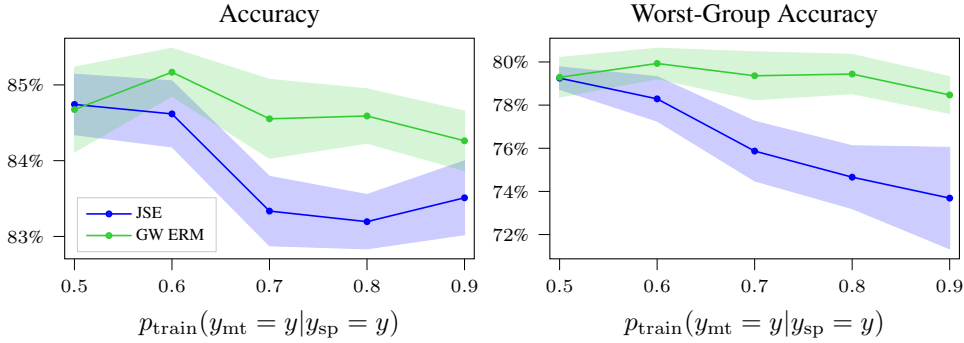


Figure 16: **Comparing JSE and group-weighted (GW) ERM for CelebA dataset:** We plot the (worst-group) accuracy on an OOD test set where $p_{\text{OOD}}(y_{\text{mt}} = y | y_{\text{sp}} = y) = 0.5$, as a function of $p_{\text{train}}(y_{\text{mt}} = y | y_{\text{sp}} = y)$. Each accuracy is obtained by averaging over 20 runs. The shaded area reflects the 95% confidence interval.

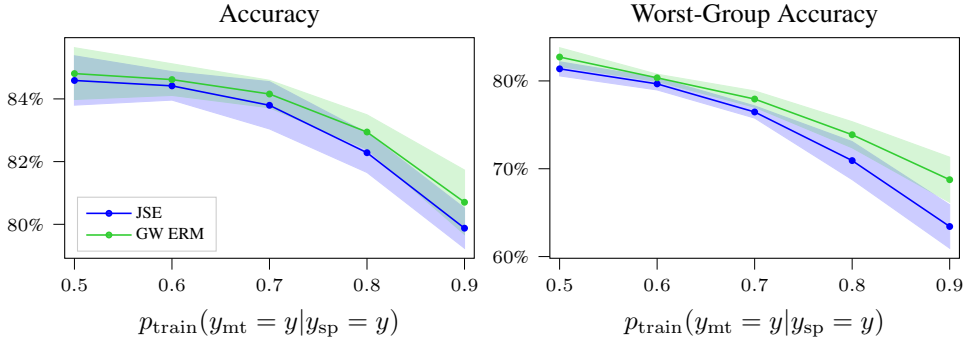


Figure 17: **Comparing JSE and group-weighted (GW) ERM for MultiNLI dataset:** We plot the (worst-group) accuracy on an OOD test set where $p_{\text{OOD}}(y_{\text{mt}} = y | y_{\text{sp}} = y) = 0.5$, as a function of $p_{\text{train}}(y_{\text{mt}} = y | y_{\text{sp}} = y)$. Each accuracy is obtained by averaging over 5 runs. The shaded area reflects the 95% confidence interval.

F DETAILS ON DATASETS, MODELS, AND PARAMETER SELECTION

F.1 DATASETS

Toy: For a given dataset size (e.g. $n = 2,000$) the data is split into an 80% training and 20% validation set, and a test set of the same size is kept apart for evaluation. We describe the data-generating process of this dataset in Section 4.1.

Waterbirds: this dataset from Sagawa et al. (2020) is a combination of the Places dataset (Zhou et al., 2016) and the CUB dataset (Welinder et al., 2010). An ‘water background’ is set by selecting an image from the lake and ocean categories in the places dataset, and the ‘land background’ is set based on the broadleaf and bamboo forest categories. A waterbird/land is then pasted in front of the background. When creating new versions of the dataset, we change the $p(y_{\text{mt}} = y | y_{\text{sp}} = y)$, and keep the size of the training set at 4,775 samples, and 1,199 for the validation set. For the test set, we select 5,796 samples where $p(y_{\text{mt}} = y | y_{\text{sp}} = y) = 0.5$.

For this dataset when training ERM or adversarial removal, we sample in each batch such that $p(y_{\text{mt}} = 1) = 0.5$. When training JSE, INLP or RLACE, we sample in each batch such that $p(y_{\text{mt}} = 1) = 0.5$. When training ERM on the embeddings transformed by JSE, INLP or RLACE, we sample again such that in each batch $p(y_{\text{mt}} = 1) = 0.5$.

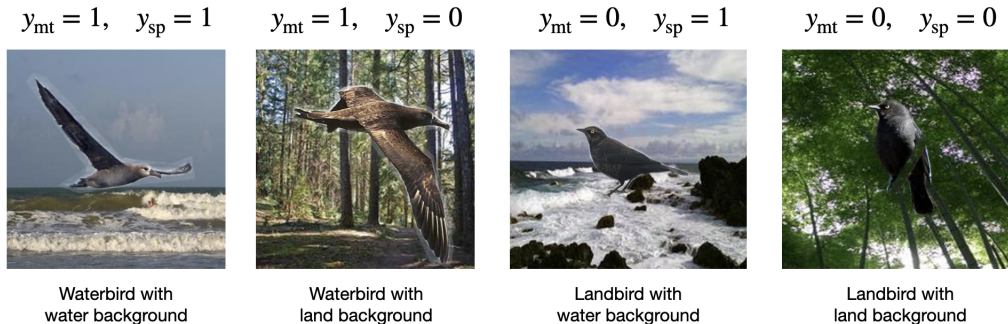


Figure 18: Examples of the different images in the Waterbirds dataset

CelebA: this dataset contains images of celebrity faces (Liu et al., 2015). The total size of the dataset is 202,599, from which we sample smaller versions. For these smaller versions, we select 4,500 observations for the training set, 2,000 for the validation set, and 2,000 for the test set. We set the $p(y_{mt} = y|y_{sp} = y)$ for the training and validation set, while we set $p(y_{mt} = y|y_{sp} = y) = 0.5$ for the test set. In the smaller versions of the dataset, $p(y_{mt} = 1) = 0.5$.

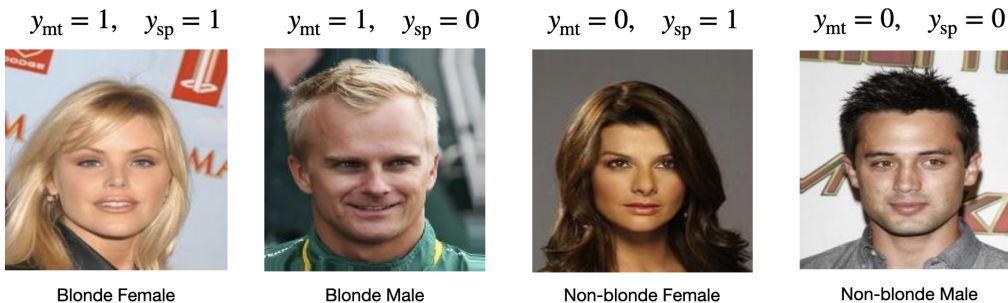


Figure 19: Examples of the different images in the CelebA dataset

MultiNLI: the MultiNLI dataset (Williams et al., 2018) contains pairs of sentences, with examples shown in Table 7. The sentences are pasted together with a [SEP] token in between. We change the dependent variable to a binary label, with $y_{mt} = 1$ indicating the first sentence (the premise) contradicting the second sentence (the hypothesis), and y_{sp} otherwise. The original dataset contains 206,175 pairs of sentences. We sample smaller versions of the dataset where $p(y_{mt} = 1) = 0.5$ and change the $p(y_{mt} = y|y_{sp} = y)$ for the training and validation set. For the test set, we set $p(y_{mt} = y|y_{sp} = y) = 0.5$.

y_{sp}	y_{mt}	Premise	Hypothesis
0	0	Conceptually cream skimming has two basic dimensions - product and geography.	Product and geography are what make cream skimming work !!
1		One of our number will carry out your instructions minutely.	A member of my team will execute your orders with immense precision.
0	1	Fun for adults and children.	Fun for only children.
1		This analysis pooled estimates from these two studies to develop a C-R function linking PM to chronic bronchitis.	The analysis proves that there is no link between PM and bronchitis !!

Table 7: Examples from sentence pairs in the MultiNLI dataset.

For simplicity, we perform no data augmentation for any of the datasets. When training logistic regressions on the last-layer representations, we demean the data based on the mean of the training

set. This is based on previous work from Chen et al. (2020), which states that demeaning is a necessary step before determining concept vectors.

F.2 MODELS & TRAINING PROCEDURE

Models: For the Waterbirds dataset, we use the Resnet50 architecture implemented in the `torchvision` package: `torchvision.models.resnet50(pretrained=True)`. More details on the model can be found in the original paper from He et al. (2016). PCA is applied to the embeddings of the layer of the architecture, to reduce the dimensionality from 2048 to 100.

For the MultiNLI dataset, we use the base BERT model implemented in the `transformers` package (Wolf et al., 2019): `BertModel.from_pretrained("bert-base-uncased")`. The model was pre-trained on BookCorpus, a dataset consisting of 11,038 unpublished books, as well as the English Wikipedia (excluding lists, tables and headers). More details on the model can be found in the original paper: Devlin et al. (2018). PCA is applied to the [CLS] embeddings, to reduce the dimensionality from 768 to 100.

Training procedure: For JSE, ERM INLP and RLACE, we use early stopping to prevent overfitting. If we observe no improvement on the validation set for a certain model after 5 epochs, the training procedure is stopped and the model with the lowest loss on the validation set is selected. We use stochastic gradient descent (SGD) with a momentum parameter of 0.9 for JSE, ERM INLP and RLACE, and train for a maximum of 50 epochs.

For finetuning the BERT model on MultiNLI we also use early stopping, and stop the procedure if we observe no improvement after 1 epoch. We use the Adam optimizer (Kingma & Ba, 2015) with the standard settings in Pytorch. When finetuning, we train for a maximum of 10 epochs, and use a batch size of 32, learning rate of 10^{-5} , and a weight decay of 10^{-4} .

For finetuning the Resnet50 model with adversarial removal, we again use early stopping, stopping if we observe no improvement after 1 epoch. We use the SGD optimizer, and train for a maximum of 20 epochs with a batch size of 128, learning rate of 10^{-3} and weight decay of 10^{-4} .

F.3 IMPLEMENTATION DETAILS & PARAMETER SELECTION

We only assume access to a validation dataset that follows the same distribution as the training dataset. This means that the conditional probability $p(y_{\text{mt}} = y | y_{\text{sp}} = y)$ is the same across the training and validation set.

For experiments where we change the $p(y_{\text{mt}} = y | y_{\text{sp}} = y)$ in the training set, we do not select new parameters for each case, but select them based on the scenario where $p(y_{\text{mt}} = y | y_{\text{sp}} = y) = 0.9$.

For JSE, ERM and INLP, we set the batch size at 128. We also do so for RLACE, except in the case of the MultiNLI dataset - we only observed convergence for this dataset and method with a batch size of 512. After setting the batch size, we select the best combination of the learning rate and weight decay. For the learning rate, we assess the values 10^{-1} , 10^{-2} , 10^{-3} and 10^{-4} . For the weight decay, we assess the values 0, 10^{-3} , 10^{-2} , 10^{-1} and 1. In the case of the Toy dataset we always set the weight decay to 0. For each method, we use the weighted binary cross-entropy on the validation set to measure performance. In the case of the toy, Waterbirds and CelebA dataset the performance is measured across 10 runs with a different seed. For the MultiNLI dataset, we measure it across 5 runs, each time finetuning the BERT model.

Below, we detail how the parameters were selected for each method, as well as implementation details for RLACE and adversarial removal. The selected combinations of the learning rate and weight decay can be found in Table 8.

ERM: We select the learning rate and weight-decay combination that has the best performance for the main-task labels. These parameters are also used when fitting a logistic regression on the transformed representations from JSE, INLP or RLACE. We keep the parameters the same for group-weighted ERM.

INLP: we select the combination of parameters that has the best performance for the spurious concept labels, based on the first spurious concept vector found by INLP. We continue projecting out the spurious concept vectors found by INLP until the accuracy of the spurious concept classifier is no

better than a majority rule classifier. Whether or not the BCE is statistically significantly different from that of a majority rule classifier is tested via an t -test of the difference in the BCE’s for both classifiers, where the critical value is determined based on $\alpha = 0.05$.

JSE: we select the combination of parameters that has the best performance for the spurious concept and main-task concept labels, weighing each equally. This performance is based on the first set of spurious and main-task concept vectors.

RLACE: we use the code from Ravfogel et al. (2022a), and run the algorithm for a maximum of 50,000 iterations. For the spurious concept classifier and optimizing the projection matrix, we use the same parameters as INLP. We optimize the projection matrix until the accuracy of the classifier is lower than 51%. Similar to Ravfogel et al. (2022a), in each case we find a matrix of rank 1.

Adversarial removal: The weight of the adversary loss is set to $\lambda = 1$. The entire architecture is finetuned, and the adversary is trained using the gradient reversal method (Ganin & Lempitsky, 2015). For the vision datasets, we observe that the accuracy of the adversary converges to below 55%, which is commonly accepted as success for the method. After the adversarial removal method, we apply standard ERM including PCA, as for the other methods.

For MultiNLI, we experimented extensively with hyper-parameters in order to get both a high accuracy on the main task, and the accuracy of the adversary to converge to below 55%. We did not observe this, even after lowering the weight of the adversary loss from 1 to 10^{-1} or even 10^{-2} . We used the Adam optimizer when performing adversarial removal.

Dataset	Method	Learning Rate	Weight Decay
Toy	JSE	10^{-2}	0
	ERM	10^{-1}	0
	INLP	10^{-1}	0
	RLACE	10^{-1}	0
Waterbirds	JSE	10^{-3}	10^{-3}
	ERM	10^{-2}	10^{-2}
	INLP	10^{-1}	10^{-3}
	RLACE	10^{-1}	10^{-3}
	ADV	10^{-3}	10^{-4}
CelebA	JSE	10^{-2}	10^{-3}
	ERM	10^{-2}	10^{-2}
	INLP	10^{-2}	10^{-3}
	RLACE	10^{-2}	10^{-3}
	ADV	10^{-3}	10^{-4}
MultiNLI	JSE	10^{-2}	10^{-2}
	ERM	10^{-2}	1
	INLP	10^{-2}	10^{-3}
	RLACE	10^{-2}	10^{-2}

Table 8: Selected combinations of learning rate and weight decay.